On Lateral Viscosity Contrast in the Mantle and the Rheology of' Low Frequency Geodynamics

by

Erik R. Ivins *
and
Charles G. Sammis

University of Southern California
Department of Earth Sciences
Los Angeles, CA 90089-0740

*ah at Jet Prepulsion Lab. / Caltech
Earth and Space Sciences Division
Pasadena, CA 91109-8099

Submitted to Geophysical J. Int.
June 22, 1994

Summary

Mantle-wide heterogeneity is largely controlled by deeply penetrating thermal convective currents. These thermal currents arc likely to produce. significant lateral variation in rheology and this can profoundly influence overall material behavior. How thermally related lateral viscosity variations impact models of glacio-isostatic and tidal deformation is large.ly unknown. An important step toward model improvement is to quantify, or bound, the actual viscosity variations that characterize the mantle. Toward this goal, two approaches arc considered. The first involves simple scaling of viscosity to shear wave velocity fluctuation. Map-views of long wavelength viscosity variation give a general quantitative description and aid in estimating the depth-dcpcndcncc of rheological heterogeneity throughout the mantle. The upper mantle is probably characterized by two to four orders of magnitude variation (Jwk-to-peak). Discrepant time scales for rebounding Holocene shorelines of Hudson Bay and southern Iceland arc consistent with this characterization. A second approach is to bound extreme negative viscosity variation by considering both seismologically based information and dynamic models of plumes, back-arcs and mirl-ocean ridges. Results arc given in terms of a local average viscosity ratio, $\Delta\bar{\eta}_i$, of volumetric concentration, ϕ_i. For the upper mantle deeper than 340 km the following reasonable limits arc estimated for $\Delta\bar{\eta} \approx 10^{-2}$; $0.01 \leq \phi \leq 0.15$. A spectrum of ratios $\Delta\bar{\eta}_i < 0.1$ at concentration level $\phi_i \approx 10^{-4}$ - 10^{-*} in the lower mantle imply a spectrum of shorter time scale deformational response modes for second degree spherical harmonic deformations of the Earth. This spectrum of spatial variation allows a purely Maxwellian viscoelastic rheology to simultaneously explain all solid tidal dispersion phenomena and long-term rebound-relate.d mantle viscosity. Composite theory of multiphase viscoelastic media is used to demonstrate. this effect.

Key Words: Mantle Viscosity, Heterogeneity, Constitutive Theory, Q, 1 xmg-Period Tides, Shear Modulus Dispersion

Submitted -- Geophysical J, Int.

1. Introduction

Recent developments in global seismic tomography provide three-dimensional views of S-wave structure throughout the mantle. *[Tanimoto 1990; Su & Dziewonski* 1991; *Su, Woodward & Dziewonski 1994].* The origin of lateral variation in seismic velocity is likely to involve both temperature and chemistry. To the extent that lateral structures arc related to temperature fluctuations, they imply corresponding fluctuation in viscosity. in this paper we explore the limit in which deviations from spherically symmetric S-wave velocity (δv_S) arise from temperature alone and can, therefore, be related to diffusion controlled creep processes. Since density and shear velocity must be related, predictions of temperature fluctuation, δT, from δv_S rel y on geoid and plate velocit y modeling *[Hager & Clayton 1989; Ricard & Wuming, 1991]. Poor* resolution of S-wave structure, poorly constrained activat ion parameters and uncertainty in lower mantle thermal structure suggests that any detailed portrayal of the. three-dimensional viscosity field is unjustified, Geodynamic models of solid tidal deformation and glacio-isostacy, however, require assessment of lateral viscosity variations at an order-of-rnagnitudc level. Map-views of a long wavelength thrcz-dime.nsional viscosity field can be constructed from simple. seal ing relations. These arc used as instructive guides. They indicate the magnitude of viscosity variability and help set criteria for estimating bounds. A significant portion of upper mantle seismic heterogeneit y is associated with features of smaller scale (< 300 km) *[Aki 1982; Gudmundsson, Davies & Clayton 1990; Dueker, Humphreys & Biasi 1993].* Some of the smaller scale features arc. resolved in the surface wave model of *Zhang & Tanimoto /1992).* This information, along with other seismic tomographic results, aid in constraining shorter wavelength viscosity anomalies. Models of magmagenesis at mid-ocean ridges, hotspots and back-arc basins arc also relevant to lower bounding the volumetric concentration and magnitude. of negative (weak) viscosity anomalies in the shallow upper mantle. So weak arc the. effective viscosities of some. parts of the mantle that their *natural* viscoelastic response time scales fal I close to many of the well-known orbitall y forced tidal periods.

Although solid Earth deformation models incorporate a viscoelastic shear modulus softening, they do so with completely ad-hoc assumptions about viscosity. Low frequency softening is usually estimated by extending seismic absorption band models across the tidal band *[Wahr & Bergen* 1986; *Mathews & Shapiro 1992].* These models arc. based on superpositions of one-dimensional analogue vise.oclastic springs and dash-porn. An exemplary Q - ω diagram is shown in Figure 1. A deficiency common to all such models is their reliance on a large number of free parameters. This absorption band construct is often referred to as the 'U - power law' for Q and shear modulus dispersion,

A major goal of geodynamics is to develop a constitutive theory that bridges seismological and glacial rebound time-scales *[Yuen & Peltier 1982; Zschau & R. Wang 1986; Körnig & Müller 1989]*. In this paper we approximate late.ral variations using a viscoelastic composite theory for multiphase media and show that the frequency-dependence of shear modulus dispersion, $\delta\mu = \mu(\omega) - \mu(\omega_o) / \mu(\omega_o)$ and intrinsic attenuation, $Q_\mu^{-1}(\omega)$, is adequately predicted across the entire tidal frequency band. The background matrix viscosity in these, mode.ls is equal to that employed in post-glacial rebound calculations.

2. Method for Long Wavelength Structure

2.1 Seismological and Flow Model Inversions

Horizontal thermal fluctuations in high Rayleigh number convection experiments reveal a depth-dependence that is, qualitatively, similar to observed velocity anomaly magnitudes in the mantle *[Honda 1987; Machetel 1990]* and this supports the notion that thermal expansivity, a, connects aspherical temperature, δT, to seismic velocity variations. All tomographic images of the upper mantle show long-wavelength structure beneath the Indian and Pacific ocean that diminishes with age away from spreading centers *[Su & Dziewonski 1991; D. Anderson, Tanimoto & Zhang 1992]*, providing further evidence that seismic anomaly and the. pattern of thermal convection arc related.

Joint inversion of seismic tomography, long-wavelength geoid, topography and plate velocity data provide some information for constraining lateral mantle structure. Ratio of anomalous local density, $\delta\rho(r,\theta,\lambda)/\rho_o(r) = dln$ p, to shear velocity, $\delta v_S(r,\theta,\lambda)/v_{S\,o}(r) = dlnv_S$ (subscript 'o' indicates horizontal average) is estimated by laboratory experiments and successful inversions. *Hager & Clayton [1989]* and *Dziewonski et al. [1993] suggest* that $dlnv_S$ */din* p may have considerable radial -dependence. Other geoid and plate velocity model inversions indicate that a radially uniform value. of $dlnv_S/dln$ p is appropriate. *Ricard & Wuming [1991]* assume $dln\mu$ / *din* p = 9.4 while *King & Masters [1992]* prefer a value of 6.0. The later value is consistent with estimates based on laboratory measurements *[D. Anderson 1987]* and theoretical models *[Isaak, 0. Anderson & Cohen 1992]*. Useful scaling constants arc:

$$c_1 \equiv dln\mu \;/\; dln\ \rho\ , \quad c_2 \equiv dlnv_S \;/\; dlnv_P\ , \tag{2.1a}$$

$$dlnv_S = (c_1 - 1)\, dln\rho / 2\ , \tag{2.1b}$$

$$dlnv_P = (c_1 - 1)\, dln\rho / (2c_2)\ . \tag{2.1c}$$

Quantification of lateral viscosity variation require.s additional scaling information having greater uncertainty than c_1 or c_2. Here only S - wave models arc considered and c_2 can be ignored.

2.2 Parameterization of Solid State Rheology

The basic assumption is that density anomalies, $\delta\rho/\rho_o$, arc. adequately related to convecting temperature, δT, through the. coefficient of thermal expansion, *a;*

$$\delta\rho(r,\theta,\lambda) = -\alpha(r)\rho_o(r)\ \delta T(r,\theta,\lambda) \qquad (2.2)$$

where r, O and λ expresses radial, latitudinal and longitudinal spatial-dependence, respectively. High temperature creep assumes a constitutive law:

$$\dot{\varepsilon} = \sigma/(2\eta_{ef}\ f)\ , \qquad (23)$$

where $\dot{\varepsilon}$ is strain-rate., σ, deviatoric stress and η_{eff} is a, generally, nonlinear effective viscosity. *For* creep controlled by dislocation motion the. effective (stress averaged) viscosity is

$$\eta_{ef\ f} = (\sigma^{1-n}/A)\ e^{G^*(P,T)/RT} \qquad (2.4)$$

where *A is* a constant, n is a power law exponent (≈ 3), G^* is the. Gibbs free activation energy, R, the Gas Constant with pressure, f', and temperature, T *[Sammis et al. 1977; Karato 1989].* Exponential-dependence occurs in all mantle creep processes wherein ionic diffusion controls rate. Using $G^* = E_* + PV^* - TS_*$ in (2.4) clarifies the temperature-dependence; introducing activation energy E_*, volume, V^*, and entropy S^*. At any mantle position, temperature may be divided into spherically symmetric part, $T_o(r)$, and a fluctuating component, $\delta T(r,\theta,\lambda) \equiv T - T_o$. Ratio, $\Delta\eta$, represents local deviation of viscosity from a global average. Defining a viscosity, $\eta_o(r)$, having spherical symmetry, and another, $\eta(r,\theta,\lambda)$, that does not, ratio, $\Delta\eta \equiv \eta/\eta_o$, becomes;

$$\Delta\eta = e^{-[a\ \delta T/T_o(T_o+\delta T)]} \qquad (2.5)$$

with $a(r) \equiv [E^*(r) + P(r)V^*(r)]/R$. Note in (2.5) that hot anomaly ($\delta T > 0$) has $\Delta\eta << 1$ while cold anomaly ($\delta T << 0$) has $\Delta\eta >> 1$. Equation (2.5) assume.s lateral variation to be dominated by temperature and not by defect chemistry. Water-related point defects *[Hobbs 1983; Karato 1989]* probably affect mantle rheology beneath back-arc basins and marginal seas sine.c subducting slabs actively dch ydrate into this environment *[Peacock* 1990]. The fact that only temperature effects arc estimated should be carefully noted, though, most of the influence of volatile. chemistry is likely to be concentrated at higher spherical harmonic order and degree than is contained in the whole mantle seismic heterogeneity model employed below.

An order of magnitude estimate of lateral viscosity variation can be obtained from

$$\log_{10}\Delta\eta(r,\theta,\lambda) \simeq \frac{\frac{2M}{c_1 - 1}\frac{a}{T_o}\left(\frac{1}{T_o}\right)\nu_{So}}{\left[1 - \frac{2}{c_1 - 1}\frac{1}{\alpha T_o}\right]} \frac{A^*\,\delta\nu_S(r,\theta,\lambda)/\nu_{So}(r)}{1 - \varepsilon_v(r,\theta,\lambda)} \qquad (2.6)$$

with $A^*(r) \equiv M\,(a/T_o)\varepsilon^*$, $\varepsilon_v(r,\theta,\lambda) \equiv$ f." $\delta\nu_S/\nu_{So}$, $\varepsilon^* \equiv 2(\alpha T_o)^{-1}(c_1-1)^{-1}$ and $M \equiv \log_{10}e = 0.4343$. Equation *(2.6)* provides insight into the depth and lateral parameter sensitivity involved. There is notable uncertainty in both the activation parameter, a, and 'DI.A' parameter c_1. Radial variation of a and $\delta\nu_S/\nu_{So}$ are estimable to within a factor of about two. However, equation *(2.6)* predicts a T_o^{-2} dependence and error in estimating T_o is of concern. Activation parameters consistent with both upper and lower mantle viscosity inversions have been discussed recently by *Ivins, Sammis & Yoder* [19931 (V'able. 1, Fig. 1, therein). Parameter c, is taken to be constant with depth, consistent with inversions for geoid and plate velocity by *Ricard & Wuming [1991].* Estimates of thermal expansivity, *a,* have been reviewed by O. *Anderson, Isaak & Oda [1992]* and experimental results with perovskite strut ture [Y. *Wang et* al. 1991; *Morishima et al. 1994]* arc. relevant to the lower mantle. Dimensionless parametcr A^* exercises stronger control than the term $(1-\varepsilon_v)^{-1}$, consequentl y,

$$\frac{A^*}{1 - \varepsilon_v(r,\theta,\lambda)} \simeq A^* \quad , \qquad (2.7)$$

simplifying (2.6) (o a linear scaling relation. For example, $A^* = -100$, implies that ν_S anomalies of 1 % correspond to 1 order of magnitude in lateral viscosity variation. While this linear approximation is useful, it becomes rather poor in the. deepest mantle and is not assumed in map-views presented below.

Perhaps a superior model for extrapolation of creep laws to depth is accomplished by replacing the ratio of activation enthalpy to temperature, H^*/RT, ($\equiv E^* + P\,V^*/RT$) with a homologous temperature, T_m/T, (T_m is the melting temperature) multiplied by a dimensionless activation energy g *[Sammis, Smith & Schubert 1981; Borch & Green 1987].* In this case

$$a(r) = g(r) \cdot T_m(r) \quad . \qquad (2.8)$$

Recent creep experiments for perovskite analogues *[Wright, Price. & Poirier 1992]* and diamond cell melting experiments for $(Mg_{.88}Fe_{.1}1)SiO_3$ at lower mantle pressures *[Zerr & Boehler* 1993] allow for a reasonable estimate of depth-independent g and depth-dcpcndcnt T_m.

3. Maps of Viscosity Variation

Models of *Tanimoto [1990]* (MDLSH), *Su & Dziewonski [1991] (S11425.2)* and *Su, Woodward & Dziewonski [1994] (S 12Wh4* 13) for $\delta v_S(r,\theta,\lambda)/v_{S0}(r)$ arc employed with (2.6) in order to produce map-views of $\Delta\eta$ at any depth in the mantle. Assuming approximation (2.7), equation (2.6) is

$$\log_{10}\Delta\eta(r,\theta,\lambda) \simeq M \frac{a}{\alpha}\frac{d\ln\rho}{d\ln v_S} T_o^{-2} \frac{\delta v_S}{v_{S0}} \quad . \tag{3.1}$$

Before discussing the map-views it is important to quantify the $T_o(r)$-dependence and decipher differences between seismic tomographic models. Physical constants used to generate depth-dcpcndcnt spherical harmonic power spectra for [wo long, wavelength seismic models arc given in Table 1. Figurc 2 shows the power spectra for two seismic models and end-member mantle geotherms $T_o(r)$ that correspond to single and [wo-layer convective simulations. Geotherms are. from *Lcitch & Yuen [1989]* ('LY s.].' in Figure 2 *b* and *c*) and from *Tackley et al. [1993]* ('T d.l.' in Figure 2a) for whole mantle and (dominantly) layered convection, respectively. Coefficients, η_{lm1} and η_{lm2} arc normalized $\cos(m\lambda)$ and $\sin(m\lambda)$ coefficients of a spherical harmonic expansion of (3.1). Figure 2 reveals the relative contributions of differences in seismic model versus differences in model $T_o(r)$. Whole mantle convective geotherms tend to be colder than those. for double,-layer, or intermittently penetrative, convection. Comparison of Figure 2 (*a*) and (b) shows that colder geotherms prc.diet stronger variation in deep mantle viscosity than dots hotter $T_o(r)$. Comparison of Figure 2 (*b*) and (*c*) reveals that seismic models also affect predictions of viscosity variability, especially in the deep lower mantle.

Figure 3 shows contours of $\log_{10}\Delta\eta(r,\theta,\lambda)$ at a 0.5 level. A value of 1.0 reveals one order of magnitude deviation from model viscosity with spherically symmetric $T_o(r)$. Figure 3 also shows the variability in model prediction using pairs of parameters *a* and $c_1(d\ln p/d\ln \rho)$ that inhibit late.ral variations (Figure 3 *a*, *b*) as opposed to those promoting $\Delta\eta$ (Figure 3 c, *d*). For example, the two thermal expansivity values assumed arc., respectively, near the differing high-temperature and high-pressure (γ phase) estimates for forsterite suggested by *O.* Anderson. *Isaak & Oda* /19921. Either of the two estimates of c, used in Figure 3 arc. consistent with geoid model inversion.

The most striking feature al 350 km depth is a coincidence of northern hemispheric viscosity maxima ($\Delta\eta \approx 102$) and the centers of the great Pleistocene ice sheet.s. At this depth rnap-view structural pattern mimics the S-wave. velocity model. In Figures 3a, *b* and *d* note the strong gradient in viscosity away from maxima in Europe and North America. The gradient is particularly strong between

the Great Lakes region and mantle beneath the southwestern coast of the United States. A strong gradient is found from Hudson Bay to the West Indies. Approximately one to two orders of magnitude decrease in viscosity is predicted from the eastern Baltic to the southern Red Sea. These upper mantle predictions are relatively unaffected by choice of seismic model. Fennoscandia and Laurentia are anomalous to great depths ≈ 700 km, though positive S- wave anomalies move toward the southeast and Fennoscandian anomaly is diminished. The southern hemisphere also has strong lateral variations at 350 km depth: Australia has higher than average. viscosity and oceanic. mantle accounting for most of the negative viscosity anomalies (Figure 3 c), *Gasperini & Sabadini [19$'9]* and *Nakada & Lambeck [1991]* have noted that long wavelength upper mantle S- wave structure and regional post-glacial shoreline emergence rates are correlated. While the present study supports this inference, the main objective here is to determine overall quantitative bounds revealed by simple scaling relationships.

Depth-dependence of lateral viscosity variability is represented by the power spectra shown in Figure 2. In the deep lower mantle S}1425.2 and S 12 WM 13 have better resolution since they use *SS* and *ScS* reflected phases. Figures 3*e* and 3*f* show predicted $\log_{10}\Delta\eta(r,\theta,\lambda)$ at a depth of 2600 km with thermal expansivity near that suggested by *Chopelas & Boehler [1992]*. Predicted peak-to-peak viscosity variations are 3 to 4 orders of magnitude. The main long wavelength features of S} 1425.2 are reflected in the higher resolution 12th degree spherical harmonic model S 12WM 13 (compare Figures 3*e* and 3*f*). *The* main inferences about the magnitude of lateral viscosity variability are little affected by employing the more highly resolved lower mantle. tomographic image S 12WM 13. Parameters assumed in Figure 3 are best-cs~irnates and are no[chosen to either maximize or minimize lateral variability in viscosity.

Maps of Figures 3*f* -- 3 h form an interesting intercomparison since all parameters are identical except those associated with high-temperature diffusion-controlled dislocation creep. While Figure 3*f* employs form (2.4) with G •/ 1", maps 3*g* and 3h employ homologous temperature form (2..8). Figures 3*f* and 3*g* , none-the,-less, produce similar $\Delta\eta(r,\theta,\lambda)$ at 2600 km depth. Comparison of maps 3g and 3*h* shows an enhanced $\log_{10}\Delta\eta(\theta,\lambda)$ magnitude induced by larger activation parameter g. The latter differ only in the assumed slip systems determined from high temperature creep experiments with perovskite $CaTiO_3$ by *Wright, Price & Poirier [199?]*.

4. Fine Scale Heterogeneity

Map-views of long wavelength viscosity allow a quantification of rheological anomaly in terms of a concentration, ϕ_i, and new ratio, $\Delta\bar{\eta}_i \equiv \langle\eta_i\rangle/\langle\eta_o\rangle$, where $< \ldots >$ is a spatial average. The value of $\langle\eta_o\rangle$ is an average of all viscosity greater than an isolated weak component $\langle\eta_i\rangle$ (see Table 2), with $\langle\eta_o\rangle > \eta_o$ and $\Delta\bar{\eta}_i < 1$. Subscript 'i' indicates multiple pairing of ratios and concentration. Soft long wavelength anomalies arc estimated to be $\log_{10}\Delta\bar{\eta} = -2 \pm 1$ at concentration level $\phi \approx 0.1 \pm 0.05$ in the upper mantle. and at top and bottom of the lower mantle. Attention is now turned toward short wavelength features with negative. velocity anomaly. These involve more extreme $\Delta\bar{\eta}$ and smaller ϕ than do long wavelength features. Two scales arc considered. First, arc those with wavelength of order $\approx$ SO - 250 km, corresponding to features that are somewhat resolved in tomographic models of the, top half of the upper mantle. Secondly, there arc smaller scale features of lateral dime.nsion $\approx$ 50 km to $\leq$ 1 km with varying degrees of partial melt content. Rock strength is reduced by partial melt. Although seismic tomography cannot be applied as in the previous section, it provides some information for constraining ϕ in the shallow upper mantle..

4.1 Lower Bound on ϕ with $\Delta\bar{\eta} < 10^{-2}$

Quantification of small scale heterogeneity is difficult and, generally, simple. scaling relation (2.6) does not apply. *Sato [1991]* combined velocity and attenuation data with empiricall y based relations to infer an asthenospheric viscosity beneath very young (O - 5 Ma) and youthful (5 - 10 Ma) oceanic lithosphere near 10^{16} and 10^{18} Pa s, respectively. A reasonable estimate in the upper mantle. is that 2-3 % negative S-wave anomalies represent 2 orders of magnitude in vise.osit y variation *[Sato J* 991].

Zhang & Tanimoto [1992] employed 75 - 250 s surface waves to construct a refined map of the, upper 500 km of the mantle and produced a spherical harmonic degree 36 model. The model images structure beneath hotspots and mid-ocean ridge.s. *Zhang & Tanimoto [1992]* showed that the mapped slow *S* -wave, area, in vertical cross-section, beneath the. ridge axes scale.d with spreading rate. For our purposes this scaling concept is useful since all ocean basin spreading rate.s arc available from global kinematic modeling *[DeMets et al. 1990]*. A detailed volume estimate can be constructed that includes sphericity, velocity structure from the degree 36 model cross-sectional areas, known oceanic ridge spreading half-rates and surface geometry. Sub-ridge mate.rial of diminished S-wave velocity of 2% (or greater) represents roughly O.] % of the mantle's volume. Only lateral contrast is considered within the oceanic LVZ with PREM *[Dziewonski & D. Anderson 1981]* as a reference model. The LVZ is likely

to represent a viscosity minimum in radial profile *[Borch & Green 1987; Mitrovica & Peltier 1993]* and, consequently, embedded viscosity anomalies are even stronger in three-dimensions. Again, this lower bound is arrived at by only considering sub-ridge. mantle S-wave structure. This lower bound can be improved upon by considerations of back-arc basins, hotspots and mantle beneath continental extensional provinces.

Mantle beneath active marginal seas and back-arc basins of the. western Pacific contain regions of S-wave anomaly at the 2 -4.5 % level *[Fukao et al.* 1992; *Hasegawa et al. 1993]*. Material beneath western Pacific marginal seas and back-arcs contributes an additional 0.1 % to the lower bound for mantle material having viscosity contrast $\Delta\bar{\eta} < 10^{-2}$ Plumes also contribute. to improving the lower bound. Numerical and analytical simulation of hotspot dynamics /Olson, *Schubert & C. Anderson 1993]* indicate that the Hawaiian plume has a viscosity reduced from surrounding mantle. by 2 to 4 orders of magnitude over short (≈100 km) lateral length scales. 'J'here arc two classes of plume.s: 24 corresponding to large oceanic hotspots *[Chase* 1985] and 18 weaker, yet classifiable, hotspots *[Duncan & Richards 15'91]*. Lower bounds for mantle fraction with $\Delta\bar{\eta} < 10^{-2}$ is raised to about 0.2- 0.S % by considering the total contribution from plumes. Asthenosphere beneath continental extensional regimes also contributes to the total lower bound, *P*-wave imagery of the western U.S. indicate.s variable. structure to depths of at least 200 km with amplitudes of ±4% *[Dueker, Humphreys & Biasi* 1993). The percentage of continental land area participating in active extension, however, is small (≈ 3- 4%), Continental extensional regimes probably contribute no more than an additional 0.1 % 10 the mantle total. Our estimate of a lower bound with $\Delta\bar{\eta} \leq 10^{-2}$ is 0.6 ± 0.3 % for the whole mantle and 1.5 ± 0.7 % for the upper mantle separately. These estimates arc obviously very crude.

4.2 *Estimate of Partial Melt Softening*

The. presence of partial melt enhances aggregate rock deformation. *Cooper & Kohlstedt [1986]* identify three mechanisms as important. The first is caused by increasing portion of hydrostatic load that can be supported by a liquid phase. At high mch fraction ($\phi_{pm} \geq 0.2$) this mechanism can cause a catastrophic decrease in strength since nearly all deformation is determined by relatively unobstructed motion of the liquid phase *[Arzi 1978; van dcr Molen & Paterson 1979]*. Other mechanisms arc effective at smaller ϕ_{pm}: crystalline interfacial sliding and creep enhancement by solution transport. These latter mechanisms arc not, however, effective at reducing viscosity by more than factors of two to live for partial melt fraction, $\phi_{pm} < 0.1$ *[Cooper & Kohlstedt 1986; Riley & Kohlstedt 1991; Beeman*

& Kohlstedt 1993]. Order 1 to 5 % melting, typical of the locus of mitt-occarr ridge asthenospheric upwell ing *[McKenzie & Bickle 1988; Forsyth J 993],* could correspond to $\eta_{eff} = 2 - 5 \times 10^{16}$ Pa s. The.sc values arc consistent with viscosities computed recently by *Scott [1993]* for mantle (plus melt) convection beneath mid-ocean ridges.

Kent, Harding & Orcutt [199.?] applied seismic. reflection methods to a segment of the East Pacific Rise. 'f ese data place tight bounds on the dimensions of the axial magma chamber. The imaged magma chamber is characterized by axial lens of 0.7 km in width and a maximum thickness of about 0.05 km. Volumetric fraction of upper mantle occupied by the, world's mid-ocean ridge axial magma chambers is $\phi \approx 10^{-8}$. Models of the surrounding axial crystalline/mcJt mush zone suggest dime.nsions of 60 km in depth extent of a conically shaped region that fans out laterally to a maximum width of about 120 - 200 km *[McKenzie & Bickle 1988; Kent Harding & Orcutt 1993]* and has an average regional partial melt fraction $\phi_{pm} \approx$ 0.0S- ().07 *[Forsyth 1993].* Wc conclude, with about an order of magnitude in uncertainty, that seismic images and flow models of the axial mush zone imply upper mantle $\phi \approx 10^{-5}$ - 10^{-4} with $\Delta\tilde{\eta} \simeq$ 106- 10"5. This is a lower bound since plume and back-arc thcr-mal-melt structures contribute in a similar manner /see *Watson & McKenzie J 991; Davies & Bickle 1991].* Here no consideration has been made for partial melting that could exist in these structures or anywhere else in (hc mantle.

5. lateral Heterogeneity as a Composite Media

Our view of lateral heterogeneity is, in essence, that the mantle contains a spatial spectrum of thermally activated creep strength. Weak parts of the space arc actually well represented by Figure 5 which is a view of $\delta v_S / v_{S_0}$ below 0.6% throughout the. mantle *[Su, Woodward & Dziewonski 1994].* Our composite models builds from the conceptual framework seen in Figure 5. Weak (slow) anomalies (Figure 5) arc viewed as a two-phase viscoelastic composite since the most intense anomalies arc not captured by global tomography. The long wave.lcngd[anomalies arc but one part of the weak phase. The surrounding mantle (unshaded in Figure 5) probably also contains weak spots and, therefore, is also modeled as a two phase viscoelastic composite. Each of the two regions arc analogies to the shaded and unshaded portions shown in Figure. 6 and arc each modeled as a generally sc.lf-consistent Maxwell viscoelastic composite. The two regions arc combined using Hashin-Shtrikman upper bounds, The basic components of each of these two regions is described in Figure 6 (also scc Appendix). Connection of scaled $\Delta\tilde{\eta}_i$ to ratios of composite theory are give in Table 2.

6. implications for Rheological Modeling of Isostacy and Low Frequency Geodynamics

6.1 Glacial Isostacy

The classical determination of mantle viscosity derives from modeling slow isostatic response to the Last Pleistocene deglaciation event. The highest quality data comes from Holocene shorelines that have large uplift amplitudes. These arc located near the centers of the Last Pleistocene glacial epoch: The Gulf of Bothnia and Hudson Bay. Below the.sc two inland seas arc Archean crust and upper mantle of relatively fast seismic velocity. One criticism of inversions for mantle viscosity that utilize shoreline. data at the.sc sites *[Haskell 1935]* is that a spatial bias is inherent. Recent inversions of Holocene shoreline data for Australia, Great Britain and south Pacific islands yield viscosity values lower than those relying more heavily on data from cratonic continental regions *[Nakada & Lambeck 1991]. Tushingham & Peltier [1992]* suggest that inversions using 392 global shorelines reveal systematic misfits to data along the cast coast of North America that could be explained by an anomalously deep mechanical lithosphere. Rapid land emergence in response to melting of Icelandic Younger Dryas (11-10 ka BP) ice sheets indicate an upper bound of 1.0 x 10^{19} Pa s for asthenospheric viscosity *[Sigmundsson 1991]*. Implied lateral variations in viscosity exceed two orders of magnitude and this is consistent with predictions that rely on long wavelength seismic tomography (MDLSH, S11425.2 and S 12 WM13) and laboratory creep measurements.

Shoreline data alone do not provide the spatial coverage necessary to distinguish between long or short wavelength interpretations of lateral rheological variation, More importantly, seismic tomography also faces the criticism that global models reflect long-arc averages of features that arc actually of smaller scale *[Gudmundsson, Davies & Clayton 1990]*. If seismic pictures of 3D structure are 'blurred', as suggested by *Machetel [1990]* (applying tomography to a numerical convection experiment), then a short wavelength interpretation of the Icelandic/Fennoscandian discrepancy is more apropos.

6.2 l,ow-frequency Geodynamics

There has been considerable effort recently to incorporate lateral variations in viscosity into flow models of the geoid *[Ritzert & Jacoby 1992]* and post-glacial rebound *[Gasperini & Sabadini 1989]*. There arc other mantle. deformations for which late.ral variations could also be important. in particular, there. arc sub-seismic oscillations caused by external tidal forcing and rotational modes such as the 434 day Chandler wobble. Solid tidal Q in this frequency range has a fairly flat response.

Onc explanation of this observation is to extend the absorption band for Iow-frequency seismic waves into the tidal band *[Smith & Dahlen 1981]*. However, in this extension to the tidal band the microphysics of attenuation and dispersion is assumed to be controlled by anelastic processes. Anelasticity is quite distinct from viscoelastic fluid rheology. In the former case as $\omega \rightarrow$ O, Q -> ∞ and the mate.rial is perfectly elastic. It is unlikely that this 'solid' rheology characterizes global deformations with periods of half a day to 18.6 years *[Karato & Spetzler 1990]*. Distinguishment between solid (anelastic) and fluid vise.oclaslic rheology (Figure. 4) in computing frequency-dcpcndcnt tidal Love numbers has, in f act, been recognized by *Yuen & Peltier [1982]* and *Dehant & Zschau [1989]*. *Sabadini, Yuen & Widmer [193'5]* employed a radial] y stratified standard linear solid (SLS) mantle model to predict tidal Love number dispersion at the 18.6 year tidal period. Although perfectl y elastic as $\omega \rightarrow$ O, the stratified S1 .S model demonstrated the importance of a weakest short-term viscosity, η_2 (see Figure 4), in a shallow 200 km thick asthenosphere.

What, then, can the concept of lateral heterogeneity add to our understanding of dispersion and dissipation at tidal frequencies? First, the deformation induced by external gravitational tides is maximum at the bottom of the lower mantle *[Smith & Dahlen 1981; Yoder & Ivins 1988]*; a region that we estimate to have enormous lateral rheological str ucture (see Figures 3*e* to 3*h*). Secondly, the weak components promote a significant shear enhancement within their interiors *and within* surrounding stronger mantle. The. weakest components of this system may bc akin to the asthenospheric S1.S η_2 modeled by *Sabadini, Yuen and Widmer [1985]* in that these readily induce a viscous softening that should bc reflected as a detectabl y large.r long-per iod tidal potential I ove number k_2.

6.3 A Role for Maxwell Viscoelastic Composite Theory

Isolated pockets of viscous fluid embedded in an elastic. medium induce a viscoclastic-like behavior when the deformation length scale is much larger that that of the inclusions. The mixture of viscous and elastic processes produces a new time-dependent behavior that neither the inclusion nor the matrix have in isolation from one. another. The mixture. creates new relaxation modes that arc induced by fluid-elastic interactions *[Frölich & Sack 1946]*. These modes can act resonantly and give substantial contribution to tidal Q and dispersion *[Ivins & Sammis* 1994]. The amplitudes of resonant behavior is determined by concentration (ϕ_i) and strength ($\Delta\bar{\eta}_i$) of heterogeneities in the media. This is well - known in the case of wave attenuation and dispersion in partially molten rocks *[Shankland, O'Connell & Waff 1981]*. For periods of oscillation in the tidal band the simple.st possible rheological assumption

is that of Maxwellian viscoelastic behavior. With such an assumption short period behavior is dominated by elasticity and long periods by Newtonian viscous flow. Maxwell mate.rials have infinite dissipation (Q^{-1}) at long period (T) and zero at $T \to 0$ (see Figure 4). Maxwell rheology captures the basic material behavior of the mantle. *[Peltier 1989]* during isostatic response to Pleistocene glacial loading and unloading (period $T \approx 103\text{-}1\,0^5$ years). The main drawback in applying homogeneous Maxwell models to solid body tides is the sharpness in predicted modulus dispersion and dissipation as a function of frequency *[Lambeck & Nakiboglu 1983]*. By considering a laterally heterogeneous viscoelastic composite rheology this sharpness in the response disappears. This conceptual breakthrough is realized only through appreciation of late.ral variability in mantle creep strength at the 2- 3 three order of magnitude level.

Although a complete derivation of a composite constitutive theory for a medium consisting of a Maxwell viscoelastic matrix with cmbcddcd Maxwell viscoelastic inclusions is beyond the scope of this paper, the main results for a multi-component theory recently developed by *Ivins & Sammis [1994)* can bc summarized as follows:

1. A generally self-consis[cmt theory for a two-phase viscoelastic media consisting of cylindrical inclusions can bc derived as a subset of a wider class of viscoelastic thin-film composites (see *Thorpe & Jasiuk [1992])* originally given by *Oldroyd [19S7].*

2. These analytic results arc combined with upper bounds on effective composite viscoelastic moduli given by *Hashin [1983].* Finite element studies of viscoelastic composites by *Brinson & Knauss* [1992] establish the accuracy of these bounds.

6.4 *Prediction of Frequency-dependent Q and* μ

Figure 7 shows predictions for Q_μ (intrinsic shear quality factor) and shear modulus dispersion ($\delta\mu$) for a hybrid model consisting of 4 phases (see Appendix A and Figure A-1). The elastic shear moduli, μ', for each of the four phases arc identical. Only the viscosity, η (scc Figure 4, top frame, and Figure 6), of the 4 phases differ in ratios that arc guided by those estimated for the manttc in Sections 3 and 4. In Figure 7 the long-short dashed line corresponds to predictions of a single two phase viscoelastic material of inclusions with viscosity ratio ${}^{(1)}R' = 10^{-5}$ at concentration ${}^{(1)}\phi = 5 \times 10^{-3}$ with a matrix viscosity ${}^{(1)}\eta = 1.0 \times 10^{22}$ Pa s. (This matrix viscosity is near a long-term a value for the lower mantle that satisfies a variety of geophysical data *[Peltier 1989; King & Masters 1992; Mitrovica*

& Peltier 1993; Ivins, Sammis & Yoder 199.?].) A second [wo-phase Maxwell viscoelastic material (type '(2)' see the long dashed line in Figure 7) is also considered. The type '(2)' composite has a lower matrix viscosity (0.5 $x10^{20}$ Pa s) and a very low viscosity ($^{(2)}\eta'$ = 1.0x 10^{16} Pa *s)* for the respective inclusion phase. Type (2) inclusion phase occurs with total concentration level 1.71% when all of type (2) phase is treated as a spherical inclusion phase to a matrix of type (1) two phase material. The exact relations for $\delta\mu$ and Q_μ are given in an Appendix. The solid line shown in Figure 7 shows the upper bound result for a 4-phase composite, Such a 4-phase composite begins to realize a fairly 'flat' attenuation spectrum (Q vs. ω) for the tidal band. The cross at the Chandler wobble (CW) frequency in Figure 7a shows an estimate based upon theory and observation *[Smith & Dahlen 1981; Okubo 1982; Wilson & Vicente 1990], In* Figure 7b the cross is at a shear modulus dispersion value determined by *Smith & Dahlen [1981]* to reconcile observed and predicted CW frequency.

Figure 8 is similar to Figure 7, the main difference being that a lower background (matrix) viscosity is assumed. Dispersion in solid Love number is primarily due to deep lower mantle shear deformation *[Smith & Dahlen 1981; Okubo 1982]*. Solid tidal potential Love number, k_2 is proportional to 'softness' or effective shear compliance. Note the significantly different $\delta\mu(\delta k_2)$ in comparing Figure 7b and 8b at the period of 18.6 years. δk_2 will come under tighter observational constraint from future satellite and VLIII-derived phase-lag and amplitude information *[Watkins & Eanes 1993]*. This geodetic data might constrain models of lower mantle rheological structure.

The broad absorption peaks that arise from lateral heterogeneity strengthen the argument that viscoelastic creep is an operative. mechanism for dispersion throughout the tidal band. Such an interpretation is in accord with microphysical attenuation mechanisms *[Karato & Spetzler 1990]*. However, all models that produce order 5% shear modulus dispersion, thus matching the *Smith & Dahlen [1981]* prediction at the Chandler period, require significant fractions ($\approx$ 10 %) of the lower mantle. to be weak by factors of 10^{-1} to 10^{-2}. The viscosity reduction is not inconsistent with scaled seismic images (Sections 2 - 4), but is larger than any lower bound on concentration that can be formulated for the lower mantle separately. A remarkable property exhibited by the simple 4-phase, viscoelastic composite is its correct prediction (solid line in Figures 7 and 8) of geodynamical behavior over such a broad frequency spectrum. We conclude that a lower mantle with background viscosity of either 10^{21} or 10^{22} Pa s that contain volumetrically significant ($\approx$ 10 %) 'soft' zones predict tidal Love number dispersion consistent with all known constraints, but that the two background values produce very different predictions of k_2 at the 18.6 year tidal period.

7. Conclusions

The goal of this paper is to provide. quantitative assessment of viscosity variability and to demonstrate its importance to physical dispersion at tidal frequencies. Uncertainty in creep mechanics is a major obstacle to obtaining reliable. viscosity estimates. It is possible, however, to construct some reasonable bounds separately for upper and lower mantle. A conservative estimate is that viscosity anomalies exist al the one to two order-of-r~)agt~il[ldc level over lateral scales of many thousands of kilometers. Scaled mantle S-wave structure has been used to estimate $\phi \simeq 0.1 \pm 0.5$ with $\Delta\tilde{\eta} \simeq 10^{n2}$. This estimate of ϕ for the upper mantle ignores the top 350 km, thus, avoiding contamination from non-thermal sources *[Boyd* 1989]. However, it is precisely in this region that thermal fluctuation is likely to be large.st since temperature advection is strongest within the thermal boundary layer of a rapidly convecting mantle. *[Jarvis & Peltier 198?; Honda 1987],* Pressure promotes viscosity variability in the deepest mantle. The volume of lower mantle with $\Delta\tilde{\eta} \leq 10^{-3}$ might be fairly large: $\phi \leq 0.01$ - 0.OS. Improved tomographic resolution could make. such estimates more reliable. Wc remark that corresponding δT in long wavelength models (Figure 2 and 3) arc consistent with values predicted for shallow upper mantle ($\geq$ 180 *'K)* by *Kaula /198.?]* and for the lower mantle ($\simeq$ 1201100 *'K) by Duffy & Ahrens [1992].* Recent computations of convective thermal fields that corrc.late with seismic observation *[Čadek et al. 1994]* indicate that lower mantle δT is substantially larger ($\simeq$ 1000 *'K)* and this strenghtens our suggestion that $\Delta\tilde{\eta} \leq$ 10-3 occurs at a 1 - 10% volumetric concentration level.

If positive velocity anomalies beneath continental shields have thermal origin the.n glacio-isostatic rebound of Laurentia and Fennoscandia sample an anomalously "stiff" upper mantle rheology with respect to global spherically symmetric average value.s. 1 ong wavelength viscosity anomalies in the shallow upper mantle explain the extremely rapid post-glacial emergence rates observed along Icelandic beaches. However, short wavelength variability might also explain the observed rate difference.

Mantle models with laterally heterogeneous viscosity arc a kcy factor in properly assessing rheology in the tidal band. A 4-phase. Maxwell viscoelastic composite rheological model provides a simpler physical description of shear modulus dispersion and attenuation at tidal frequency than do '$\tilde{\alpha}$ - power law* models. We suggest that laterally heterogeneous Maxwell viscoelasticity may be a viable constitutive relation for periods as short as 12 hours and as long as a Milankovich cycle (O 100,OW yr). Future geodetic solutions for solid body tidal Love number dispersion (δk_2) might be used to constrain deep mantle lateral variation in viscosity.

Acknowledgements

Many thanks are due Joy Crisp for comments on a very early version of this paper, to Toshiro Tanimoto for discussions on S- wave models, to Charles F. Yoder for insights concerning the observational bound on k_2 and to Richard Gross for insights on Chandler wobble Q. This research was supported by the LAGEOS II Project and by the NASA Geophysics Program. The work was performed at U.S.C's Department of Geological Sciences and at the Jet Propulsion Laboratory, California Institute of Technology, in the Earth and Space Science Division.

Appendix — Theoretical Attenuation and Dispersion

Below a brief sketch of the solutions for modulus dispersion ($\delta\mu$) and quality factor (Q_μ) for two-phase and four-phase Maxwellian viscoelastic media is given.

Two-Phase Maxwell Viscoelasticity

The two-phase media is derived from generalized self-consistcrr[theory *[Christensen 1990]*. A detailed derivation is given by *Ivins & Sammis [1994]*. The moduli arc derived on the basis of a composite cylindrical assemblage. A 'cmss-fiber' shearing component (see Figure 6) is relevant to modeling mantle shear modulus dispersion. The inclusions and the matrix are. compressible Maxwell viscoelastic with tbc same definition for viscoelastic compressibility as in *Peltier [1989]*. The concentration, ϕ, of the inclusions is dilute and there arc no explicit interactions among inclusions. In a generally self-consislcnl scheme the moduli arc. derived through a 'weak' interaction hypothesis. This 'weak' interaction limit applies to all length scales of heterogeneity, provided tbc latter arc. much smaller than a characteristic wavelength of the macroscopic deformation. This approximation is certainly realized in the case of $l=2$ deformation: the dominant mode of solid body tide.s.

The composite moduli arc analytically tractable in the case when elastic bulk modulus, κ^e and shear modulus, μ^e, arc. identical. The elastic properties appear in the relations for viscoelastic moduli as a single ratio, $\nu \equiv \kappa^e/\mu^e$. The only difference between the inclusions and matrix is the Newtonian viscosity of the analogue dashpot element (see Figure 4a). Thus, the composite moduli arc expressed in terms of a ratio $R \equiv \frac{\eta'}{\eta}$ where. η' and η arc. the. viscosity of the inclusion and matrix phases. The creep function, Y', in constitutive theory provides a nearly complete description of basic rheological properties *[see Kanamori & D. Anderson, 1977 and references therein; Christensen 1982; Körnig & Miller 1989]*. For the two-phase viscoelastic material under discussion the creep function is:

$$Y'(f) = \Theta_0(\nu,\phi) + \Theta_1(R,\phi)\, t + \Theta_2(\nu,R,\phi)\, e^{-\lambda_{slow}(\nu,R,\phi)\, t} + \Theta_3(\nu,R,\phi)\, e^{-\lambda_{fast}(\nu,R,\phi)\, t}, \quad \text{(A-1)}$$

where λ_{slow} and λ_{fast} arc. transient Lime scales for response to a Heavyside step function increase in shear stress at t = O *[Christensen 1982, Chapter 1; Ivins & Sammis 1994]*. The term linear in t represents a Newtonian viscous-like response and equation A-1 c.valuated at t = O gives the instantaneous elastic shear strain response to a unit shear load. In equation A-1 time is dime.nsionlcss with a scale, η/μ^e: the

so-called Maxwell lime for the matrix material. Coefficients Θ_i arc given in Tables A-1 and A-2. Parameters given in Table A-1 arc. coefficients of higher order time-opcralors of the viscoelastic composite: a_n's and b_n's arc associated with Maxwellian stress and strain operators, respectively. For isostacy and tidal dispersion, an important mode is associated with the. 'fast' decay lime, 1/&,$,. Another time scale, $1/\lambda_{slow}$, results from a 'slow' reaction, The latter mode is associated with deformation of boundaries of the. heterogeneities and is controlled by the stiffer viscosity, η, of the matrix. (The theory is equally valid for stiff inclusions and in this case $1/\lambda_{fast}$ is a not a fast decay time). The fast decay mock represents the ability of a sofl heterogeneity to more easil y deform. The overall amplitude of this mode of deformation is sensitive to the concentration, ϕ. A complete discussion of the.sc modes is given by *Ivins & Sammis [1994].*

The Fourier transformed shear modulus, μ, for this two-phase rheology is:

$$\mu(i\omega) = \int_0^\infty \mu_D \; e^{-i\omega t} \; dt \tag{A-2}$$

$$= \frac{i\omega\left[b_1 + i\omega b_2 - \omega^2 b_3\right]}{\left[a_1 + i\omega a_2 - \omega^2 a_3\right](1 + i\omega)}$$

where μ_D is the. time-operator shear modulus:

$$\mu_D = \frac{\sum_{n=0}^{2} b_{n+1} D^{(n+1)}}{\sum_{n=0}^{2} a_{n+1} D^{(n)} \left[1 + D^{(1)}\right]}$$

with $D^{(n)} = d^n/dt^n$ *[Ivins & Sammis 1994; Christensen 19$'2].* The Fourier transformed constitutive relation is

$$\tau = 2 i\omega \mu(i\omega) \varepsilon \tag{A-3}$$

and with equation A-2 a phase-lagged shear strain response ε that follows the stress τ by angle $\arctan(Q_\mu^{-1})$. The symbol indicates half-sided Fourier transform as in equation (A-2). The inverse of the quality factor is

$$Q_\mu^{-1} = \tag{A-4}$$

$$\frac{1}{\omega} \cdot \left[\omega^2 (b_2/b_3) A(\omega) + B(\omega) C(\omega)\right] \cdot \left[A(\omega) C(\omega) - (b_2/b_3) B(\omega)\right]^{-1}$$

where

$$A(\omega) \equiv a_2 + a_1 - \omega^2 a_3 \quad , \qquad B(\omega) \equiv a_1 - \omega^2 (a_2 + a_3)$$

$$C(\omega) \equiv (b_1 / b_3) - \omega^2 \quad .$$

The frequency-dependent complex shear modulus is $\mu^* \equiv i\omega\mu$ whose real part,

$$\mu(\omega) \equiv \mathrm{Re}\left\{ \mu^*(i\omega) \right\} \quad , \tag{A-5}$$

is the effective low frequency shear modulus.

A 4-Phase Model with Hashin-Shtrikman Bounds

Using an explicit finite element simulation of composite viscoelastic materials, *Brinson & Knauss [1992]* recently demonstrated that variational upper bounds provide a reasonably accurate prediction of modulus dispersion for a situation in which a 'stiff' matrix surrounds a set of 'soft' inclusions. The Hashin-Shtrikman (H-S) upper bounds then are appropriate to a more complicated composite rheology involving four phases instead of the two-phase composite that has been discussed so far. It allows a fundamental step to be taken toward realistic assessment of the frequency-dependence of Q_μ and shear modulus dispersion $\delta\mu$ in light of seismic constraints on lateral heterogeneity and thermal convective simulations of mantle dynamics. A four-phase model is constructed from the two phase model as discussed in Section 5. *Hashin [1983] gives* relations for bounds on the shear modulus for both cylindrical and spherical inclusions. We find that the assumed shape has little impact on the overall results.

Expressions that use H-S bounds are indicated by superscript '*HS*'. The H-S upper bound on the complex shear modulus μ^* for spherical inclusions is

$$\mu^{HS} = {}^{(2)}\mu^*(i\omega) + \tag{A-6}$$

$$\frac{1}{{}^{(1)}\mu^*(i\omega) - {}^{(2)}\mu^*(i\omega)} + \frac{(1 - {}^{(2)}\nu)}{6\,{}^{(2)}\nu\,(\kappa + 2\,{}^{(2)}\mu^*(i\omega))} \Bigg/ \frac{}{5\,{}^{(2)}\mu^*(i\omega)\,(3\kappa + 4\,{}^{(2)}\mu^*(i\omega))} \quad ,$$

where the type "2" material is a two-phase inclusion of volume fraction ${}^{(2)}\nu$ embedded in a two-phase matrix of volume fraction ${}^{(1)}\nu$ with ${}^{(1)}\nu + {}^{(2)}\nu = 1$ (see Figure A-1). The bulk modulus is assumed to be dissipation free and equal in all four phases under consideration. Finally, we note:

$$Q_{\mu}^{HS} = \mathrm{Re}\left\{\mu^{HS}(i\omega)\right\} \Big/ \mathrm{Im}\left\{\mu^{HS}(i\omega)\right\} \quad . \tag{A-7}$$

In order to apply the bound given by (A-6) the complete constitutive equation for the composite viscoelastic media occupying volume space $^{(2)}v$ must be considered, in light of the common reference time scale, η/μ^e, shared with viscoelastic composite occupying volume $^{(1)}v$. The complex shear modulus, $^{(2)}\mu^*(i\omega)$, uses a slightly modified form for the frequency-dcpcndcrr[functions identified in the two-phase model. in particular, it is required that

$$^{(2)}A(\omega) = {}^{(2)}a_2 {}^{/(2)}R + {}^{*)}{}_1 - \omega^2 \quad {}^{'2)}(13 \quad ,$$

$$^{(2)}B(6)) = {}^{(2)}a_1 {}^{/(2)}R - \omega^2 ({}^{(2)}a_3 {}^{/(2)}R + {}^{(2)}a_2) \; . \tag{A-8}$$

In addition, $^{(1)}C(\omega)$ and $^{(2)}C(\omega)$ differ by their implicit dependence on different internal concentrations, $^{(1)}\phi$, $^{(2)}\phi$ and viscosity ratios, $^{(1)}R$, $^{(2)}R'$. Two new viscosity ratios arc introduced as

$$^{(2)}R \equiv \frac{^{(2)}\eta}{^{(1)}\eta} \quad , \qquad\qquad ^{(2)}R' \equiv \frac{^{(2)}\eta'}{^{(2)}\eta} \quad , \tag{A-9}$$

and material of type 1 has a corresponding ratio $^{(1)}\eta'/{}^{(1)}\eta$ that simply rc.places R. For material of type 1 the constitute vc coefficients in I'able A-1 remain unchanged, while for material of type 2 has R replaced by $^{(2)}R'$ arrd each time derivative of the operator form of the constitutive equation contains a multiplicative resealing $'^{*)}R^{p}$ where p is the order of the time derivative. In other words, each $^{(2)}a_p$ and $^{(2)}b_p$ contain multiplicative coefficients $^{(2)}R^{p}$ in contrast to those for type 1 given in Table A- 1. The minor differences arise solely from the necessity for a common reference time scale. for adjoining composite. vise.oc.laslic fluids of types 1 and 2.

The concentration, $^{(2)}v$, of two-phase viscoelastic fluid of type 2 is relatively unrestricted since the }1-S bounds are a non-dilute theory *[Brinson & Knauss* 1992]. Our models of mantle shear modulus (Figures 7 and 8) take advantage of this fact. The full range of models for Love number dispersion in the tidal band must consider lateral viscosity contrast at levels exceeding the lower bounds determined in this paper. This will be particularly apropos for models of the D'' layer.

References

Aki, K., Three-dimensional seismic inhomogeneities in the lithosphere and asthenosphere: evidence for decoupling in the. lithosphere and flow in the asthenosphere, Rev. *Geophys. Sp. Phys., 20,* 161-170. 1982.

Anderson, D.L., A seismic equation of state: II. Shear properties and thermodynamics of the lower mantle, *Phys. Earth Planet. Inter., 45,* 307-3?3, 1987.

Anderson, D.L. andJ.W.Given, Absorption hand Q model for the Earth, *J. Geophys. Res., 87, 3893-3904, 1982.*

Anderson, D.L., T. Tanimoto and Y-S. Zhang, Plate tectonics and hotspots: The third dimension, *Science,* 2S6, 1645-1651, 1992.

Anderson, O.L., D. Isaak and H. Oda, High-temperature elastic constant data on minerals relevant to geophysics. *Rev. Geophys., 30,* 57-90, 1992.

Arzi, A. A., Critical phenomena in the rheology of partially melted rocks, *Tectonophysics, 44, 173-184,* 1978.

Beeman, M.L. and D.L. Kohlstedt, Deformation of fine-grained aggregates of olivine plus melt at high temperatures and pressures, *J. Geophys. I/m., 98,* 6443-6452, *1993.*

Borch, R.S. and H.W. Green, Dependence of creep in olivine on homologous temperature and its implications for flow in the. mantle, *Nature, .?.?0, 345-348,* 1987.

Boyd, F. R., Compositional distinction between oceanic and cratonic lithosphere, *Earth Planet. Sci. Lett.,* 96, 15-26, 1989.

Brinson, L.C. and W.G. Knauss, Finite element analysis of multiphase viscoelastic solids, *J. Appl Mech., 59, 730-737,* 1992.

Cadek, O., D.A. Yuen, V. Steinbach, A. Chopelas and C. Matyska, Lower mantle. thermal structure deduced from seismic tomography, mineral physics and numerical modeling, *Earth Planet. Sci. Lett., 121,* 385-402, 1994.

Chase, C. G., The geological significance of the geoid, *Ann Rev. Earth Planet. Sci., 1.?, 97-117,* 1985.

Chopelas, A. and R. Boehler, Thermal expansivity in the lower mantle, *Geophys. Res. Lett.,* 19, 1983-*]986, 1992.*

Christensen, R.M., *Theory of Viscoelasticity: An Introduction,* Academic, New York, N. Y., pp. 364, *1982.*

Christensen, R, M., A critical evaluation for a class of micromechanics models, *J. Mech Phys. Solids,* 38, 379-40-1, 1990.

Cooper, R.F. and 1).1.. Kohlstedt, Rheology and structure of olivine-basalt partial melts, *J. Geophys. Res., 91, 9315-9323,* 1986.

Davies, J.H. and M.J. Bickle, A physical model for the volume and composition of melt produced by hydrous fluxing above subduction zones, *Phil. Trans.. R. Sot. London,* 33.5, *Ser. A,* 355-364, 1991.

Dehant, V. and J. Zschau, The effect of mantle anelasticity on tidal gravity: A comparison between spherical and elliptical Earth model, *Geophys.* l., 97, 549-S5S, 1989.

DeMets, C. R.G. Gordon, D.F. Argus and S. Stein, Current plate motions, *Geophys. J. Int., 101,* 425-478, 1990.

Ducker, K., E. Humphreys and G. Biasi, Teleseismic imaging of the western United States upper mantle structure using the simultaneous iterative reconstruction technique, in *Seismic Tomography: Theory and Practice (cd.* H.M. Iyer and K. Hirahara) Chapman and Hall, London, 265-298, 1993.

Duffy, T.S. and T.J. Ahrens, Sound velocities at high pressure and temperature and their geophysical implication, *J. Geophys. Res.,* 97, 4503-4520, 1992.

Duncan, R.A. and M.A. Richards, Hotspots, mantle plumes, flood basalts, and true polar wander, Rev. *Geophys.,* 29, 31-50, 1991.

Dziewonski, A.M. and D.L. Anderson, Preliminary reference Earth model, *Phys. Earth Planet. Inter.,* 2S, 297-356, 1981.

Dziewonski, A. M., A.M. Forte, W.-J. Su and R.J.. Woodward, Seismic tomography and geodynamics, in, *Relating Geophysical Structures and Processes, The Jeffreys Volume, Geophys. Monograph 76,* (cd, K. Aki and R. Dmowska) A.G.U., Washington. D. C., 67-105, 1993.

Forsyth, D. W., Crustal thickness and the average. depth and degree of melting in fractional melting models of passive flow beneath mid-ocean ridges, *J. Geophys. Res., 96',* 16,073-16,079, *1993.*

Frölich, } 1, and R. Sack, Theory of (he. rheological properties of dispersions, *Proc. Roy Sot. London A, 183, 415-430, 1946.*

Fukao, Y., M. Obayashi, H. Inoue and M, Nenbai, Subducting slabs stagnant in the transition ?.one, *J. Geophys. Res., 97, 4809-4822,* 1992.

Gasperini, P. and R. Sabadini, Lateral heterogeneities in mantle viscosity and post-glacial rebound, *Geophys. J., 98, 4] 3-428,* 1989.

Gudmundsson, O., J.H. Davies and R.W. Clayton, Stochastic analysis of global lravcl-time data: mantle heterogeneity and random errors in the ISC data, *Geophys. J. Int., 102, 25-43, 1990.*

Gueguen, Y., M. Darot, P. Mazot and J. Woirgard, Q^{-1} of forsterite single crystals, *Phys. Earth Planet. Inter., 55, 2S4-258,* 1989.

Hager, B.H. and R. W. Clayton, Constrains on the structure of mantle convection using seismic observations, flow models, and the geoid, in *Mantle Convection, cd.* W.R. Peltier, Gordan and Breach, N. Y., 657-763, 1989.

Hasegawa, A., A. Yamamoto, D. Zhao, S. Hori and S. Horiuchi, Deep structure of arc volcanos as inferred from seismic observations, *Phil. Trans. R. Sot. London A,* 342, 167-178, 1993.

Hashin, Z., Analysis of composite materials - A survey, *J. Applied Mechanics, 50,481-505, 1983.*

Haskell, N. A., The motion of a viscous fluid under a surface load, *Physics,* 6, 265-269, 1935.

Hobbs, B.E., Constraints on the mechanism of deformation of olivine imposed by defect chemistry, *Tectonophysics, 92, 35-69, 1983.*

Honda, S., The RMS residual temperature in the convecting mantle and seismic heterogeneities, *J. Phys. Earth, 35,* 195-207, 1987.

Isaak, D. G., O.L. Anderson and R. Ii. Cohen, The relationship between shear and compressional velocitics at high pressures: Reconciliation of seismic tomography and mineral physics, *Geophys. Res. Lett., 19, 741-744, 1992,*

Ivins, E.R. and C.G. Sammis, Q and dispersion from 10 to 10,000 nHz: Composite vise.oclastic constitutive theory for a strongly heterogeneous mantle, manuscript to be submitted to *Geophys. J. Int.,* 1994.

Ivins, E.R., C.G. Sammis and C.F. Yoder, Deep mantle viscous structure with prior estimate and satellite constrain, *J. Geophys. Res.,* 98, 4579-4609, 1993.

Jackson, 1., M.S. Paterson and J.D. Fitz Gerald, Seismic wave dispersion and attenuation in Ahcim dunite, *Geophys. J. Int., 108,* 517-539, 1992.

Jarvis, G.T. and W. Il. Peltier, Mantle convection as a boundary layer phenomenon, *Geophys. J. R. Astr. Sot., 68,* 389-427, 1982.

Kanamori, H. and D.L. Anderson, Importance of physical dispersion in surface wave and free oscillation problems, *Rev. Geophys. Sp. Phys., 15,* 105-112, 1977.

Karate, S-1., Defects and plastic deformation in olivine, Chapter 11 in, *Rheology of Solids and of the Earth, cd., S.* Karato and M. Toriumi, Oxford University Press, 177-208, 1989.

Karate, S-I. and H.A. Spetzler, Defect microdynamics in mineral physics and solid-state. mechanisms of seismic wave attenuation and velocity dispersion in the mantle, *Rev.* Geophysics, 28 399-421, 1990.

Kaula, W. M., Minimal upper mantle temperature variations consistent with observed heat flow and plate velocities, *J. Geophys. Res.,* 88, 10,323-10,332, 1983.

Kent, G.M., A.J. Harding and J.A. Orcutt, Distribution of magma beneath the East Pacific Rise between the Clipperton Transform and the. 9°17′Deval from forward modeling of common depth point data, *J. Geophys. Res., 98, 13,945-13,969, 1993.*

King, S.D. and G. Masters, An inversion for radial viscosity structure using seismic tomography, *Geophys. Res. Lett., 19,]551 -15.S4,* 1992.

Körnig, M. and G. Müller, Rheological models and interpretation of post-glacial uplift, *Geophys. J. Int., 98,* 243-253, 1989.

Lambeck, K. and S .M. Nakiboglu, Long-period Love numbers and their frequency dependence due to dispersion effects, *Geophys. Res. Lett., 11,* 857-860, 1983.

Leitch, A.M. and D.A. Yuen, Internal heating and thermal constraints on the mantle, *Geophys. Res. Lett.,* 16, 1407-1410, 1989.

Machetel, P., Short-wavelength lower mantle seismic velocity anomalies, *Geophys. Res. Lett., 17,* 1145-1148, 1990.

McKenzie, D. and M.J. Bickle, The volume and composition of melt generated by extension of the lithosphere, *J. Petrology,* 29, 625-679, 1988.

Mathews P.M. and 1.1. Shapiro, Nutations of the. Earth, *Ann. Rev. Earth Planet. Sci., 20, 469-500,* 1992.

Mitrovica, J .X. and W.R. Peltier, The inference of mantle viscosity from an inversion of the Fennoscandian relaxation spectrum, *Geophys. J. Int.,* 114, 45-62, 1993.

Morishima, H., E. Ohtani, T. Kate, O. Shimomura and T. Kikegawa, The.rmal expansion of $MgSiO_3$ at 20.5 GPa, *Geophys. Rcs. Lett.,* 21, 899-902., 1994.

Nakada, M. and K. Lambeck, Late Pleistocene and Holocene sca-level change; Evidence for lateral mantle viscosity structure ? in *Glacial Isostacy, Sea-Level and Mantle Rheology,* (ed. R. Sabadini) Kluwer, Netherlands, 79-94, 1991.

Okubo, S., Theoretical and observed Q of the Chandler wobble - I ,0vc number approach, *Geophys. J. Roy. As(r. Sot., 71 647-6S7,* 1982.

Oldroyd, J. G., The rheology of some two-dimensional disperse systems, *Camb. Phil. Sot. Proc., S.?, 514-524, 1957.*

Olson, P., G. Schubert and C. Anderson, Structure of axisymmetric mantle plumes, *J. Geophys. Res., 98,* 6829-6844,1993.

Peacock, S. M., Fluid processes in subduction zones, *Science, 248, 329-337, 1990.*

Peltier, W.R., Mantle viscosity, in *Mantle Convection, (cd.,* W.R. Peltier) Gordan & Breach, New York, 389-478, 1989.

Ricard, Y. and B. Wuming, Inferring the viscosity and the 3-D density structure of the. mantle from geoid, topography and plate velocity, *Geophys. J. Int., 105,* 561-571, 1991.

Riley, G.N. and D.L. Kohlstedt, K inetics of melt migration in upper mantle-t ypc rocks, *Earth Planet. Sci. Lett.,* 10.5, 500-521, 1991.

Ritzert, M. and W.R. Jacoby, Geoid effects in a convecting system with lateral viscosity variations, *Geophys. Res. Lett.,* 19, 1547-15S0, *1992.*

Robertson, 1>. S., J.R. Ray and W.E. Carter, Tidal variations in UT 1 observed with very long baseline interferometr y, *J. Geophys. Res., 99, 621-636, 1994.*

Sabadini, R., D.A. Yuen and R. Widmer, Constrains on shor[-term mantle rheology from the $\dot{J}_2$ observation and the dispersion of the 18.6 y tidal Love number, *Phys. Earth Planet. Inter., 38, 235-249, 1985,*

Sammis, C. G., J.C. Smith, G. Schubert and D.A. Yuen, Viscosity-depth profile of the Earth's lower mantle: effects of polymorphic phase transitions, *J. Geophys. Res.,* 82, 3747-3761, 1977.

Sammis, C.(i., J.C. Smith and G. Schubert, A critical assessment of the estimation methods for activation volume, *J. Geophys. Res., 86,* 10,707-10,718, 1981.

Sam, H., Viscosity of the upper mantle from laboratory creep and anelasticit y measurements in peridotite at high pressure and temperature, *Geophys. J. Int., 105, 587-599, 1991.*

Shankland, T. J., R.J. O'Connell and H.S. Waff, Geophysical constraints on partial melt in the upper mantle, Rev. *Geophys. Sp. Phys., 19, 394-406, 1981.*

Sigmundsson, F., Post-glacial rebound and asthenospheric viscosity in Iceland, *Geophys. Res. Lett.,* 18, 1131-1134, 1991.

Scott, D.R., Small-scale convection and mantle melting beneath mid-ocean ridges, in *Mantle Flow and Melt Generation at hliri-Ocean Ridges, Geophysical Monograph 71,* (cd. J .P. Morgan, D.K. Blackman and J.M. Sinton) A.G.U., Washington, D. C., 327-352, 1993.

Su, W-J. and A.M. Dziewonski, Predominance of long-wavelength heterogeneity in the mantle, *Nature, 352, 121-126,* 1991.

Su, W-J., R.L. Woodward and A.M. Dziewonski, Degree 12 mode.1 of shear velocity in the mantle, *J. Geophys. Res., 99,* 6945-6980, 1 994.

Tackley, P.J., D.J. Stevenson, G.A. Glatzmaier and G. Schubert, Effects of an endothermic phase. transition at 670 km depth in a spherical model of convection in the Earth's mantle, *Nature, 361, 699-704, 1993.*

Tanimoto, T., Long wavelength S-wave structure throughout the mantle, *Geophys. J., 100,* 327-336, 1990.

Thorpe, M.F. and 1. Jasiuk, New results in the theory of elasticit y for two-dimensional composites, *Proc. R. Sot. Lond. A, 438,* 531-S44, 1992.

Tushingham, A.M. and W.R. Peltier, Validation of the ICE-3G model of Wurm-Wisconsin deglaciation using a global data base of relative sea level histories, *J. Geophys. Res.*, 97, 3285-3304, 1992.

van der Molen, I. and M.S. Paterson, Experimental deformation of partially-melted granite, *Contrib. Mineral. Petrol., 70, 299-318,* 1979.

Wahr, J.M. and Z. Bergen, The effects of mantle anelasticity on nutations, Earth tides and tidal variations in rotation rate, *Geophys. J. R. Astron. Sot., 87, 633-668, 1986.*

Wang, Y., D.J. Weidner, R.C. Liebermann, X. Liu, J. Ko, M.T. Vaughn, Y. Zhao, A. Yeganeh-Haeri and R.E.G. Pacalo, Phase transition and thermal expansion of $MgSiO_3$ perovskite, Science, *251,* 410-413, 1991.

Watson, S. and D. McKenzie, Melt generation by plumes: A study of 1 lawaiian volcanism, *J. Petrology,* 32, 501-537, 1991.

Watkins, M.M. and R.J. Eanes, 1 ong term changes in the Earth's shape, rotation and geocenter, *Adv. Space Res., 13,* 251-255, 1993.

Wilson, C. Il. and R.O. Vicente, Maximum likelihood estimates of polar motion, in *Variations in Earth Rotation, Geophys. Monograph 59,* I.U.G.G. Vol. 9 (cd. D.D. McCarthy and W .E. Carter) A.G.U., Washington D. C., 151-155, 1990.

Wright, K., G.D. Price and J .P. Poirier, High-temperature creep of the perovskites $CaTiO_3$ and $NaNbO_3$, *Phys. Earth Planet. interiors, 74, 9-22, 1992.*

Yodcr, C.F. and E.R. Ivins, On the ellipticity of the core-man[lc boundary from Earth nutations and gravity, in *The Earth's Rotation and Reference Frames for Geodesy and Geodynamics, IAU Symposium 128,* ed., A. Babcock and G Wilkins, pp. 317-322, Kluwer, Boston. Mass., 1988.

Yuen, D.A. and W.R. Peltier, Normal modes of the viscoelastic Earth, *Geophys. J.* R. *Astr.* Sot., 69, 495-526, 1982.

Zerr, A. and R. Boehler, Melting of $(Mg,Fe)SiO_3$ - Perovskite to 625 kilobars: Indication of a high melting temperature in the lower mantle, *Science,* 262, 553-555, 1993.

Zhang, Y-S., and T. Tanimoto, Ridges, hotspots and their interaction as observed in seismic velocity maps, *Nature, 355, 4S-49, 1992.*

Zschau, J., and R. Wang, Imperfect elasticity in the Earth's mantle: implications for Earth tides and long period deformations, in *Proceedings of the 10th International Symposium on Earth 7'ides,*

(cd. R. Vieira) Consejo Superior de Investigaciones Cientificas, Madrid, 379-384, 1986.

Figure Captions

Figure 1. Q - ω diagram for '$\bar{\alpha}$ power law'. Inset shows typical shear modulus and Love number (k_2) dispersion. Applications to seismic data involve radially -dependent amplitudes (Q inside the absorption band) and cut-off frequencies (ω_1 and ω_2) *[D. Anderson & Given 1982]. The* cross shows how such a model could satisfy a specific Q value at the Chandler wobble. frequency.

Figure 2. Power spectra of $\log_{10}$ viscosity variation. Normalized coefficients η_{lmi} arc related to seismic velocit y coefficients by proportionality y factor given in equation (3.1). Depth-dcpcndcnt parameters arc summarized in Table 1. The normalization convention is the same as adopted by *Tanimoto [1990]* (MDLSH) and *Su & Dziewonski [1991]* (also see *Ivins, Sammis & Yoder [1993]).*

Figure 3. $\log_{10}\Delta\eta(r,\theta,\lambda)$ in mid-upper mantle (a-d) and deep lower mantle (e –h). *Seismic* models arc S}1425.2 *[Su & Dziewonski 1991],* MDLSH I *[Tanimoto 1990]* and S 12WM 13 *[Su, Woodward & Dziewonski 1994].* For frames *a*-~ equation (2.6) applies with parameters given in Table 1. Different 'DLA' - α pairs arc contrasted in a, b, c and d. In all cases $T_0(r)$ corresponds to a convective simulation of *Tackley et al. [1993).* Frames e and f compare variability for lower mantle just above D'' with two long-wavelength solutions. Frames g and h assume homologous temperature T/T_m = 0.417 (from *Zerr & Boehler [1993]*) while the dimensionless activation parameter g = 15.2 (g) and g = 22.0 (h) correspond to the perovskite $CaTiO_3$ {*100*} and {*110*} dislocation slip systems, respectively, as determined by *Wright, I'rice & Poirier [1992]. (These* values of g arc with respect to T_m at 700 km depth as determined by *Zerr & Boehler [1993]*). All contour intervals arc 0.5. The 'zero' contour corresponds to a solid line.

Figure 4. Q^{-1} - T diagrams (inverse. quality factor versus period of oscillation) for onc-dime.nsional spring-dashpot analogues rheologies. The diagrams only show qualitative features. The Maxwell and Burgers models arc viscoelastic fluid models while Kelvin-Voigt and standard linear substances arc viscoelastic, or 'anelastic', solids. The latter to not exhibit long-term creep behavior. The seismic absorption band is typically formulated as a superposition of standard linear elements whose properties arc 'solve.-for' parameters.

Figure 5. Volumes with -0.6 %, or greater, anomalously slow S - waves throughout the mantle. (From *Su, Woodward & Dziewonski [1994]* - model S 12WM 13).

Figure 6. I'wo-phase. composite model. Viscoelastic composite moduli (shear operator: μ^* , and bulk compression operator: κ^*) arc analytically related to the inclusion and matrix Maxwell viscoelastic moduli (η, κ' and μ') with and without primes, respectively. A generally self-consistent scheme evaluates composite. operators from a solution at boundary ζ. For two dimensions this is a three.-phase cylinder model *[Christensen 1990]* (see Appendix for further discussion).

Figure 7. Predicted $Q_\mu(\omega)$ (a) and $\delta\mu \equiv [\mu(\omega) - \mu(\omega_o)] / \mu(\omega_o)$ (b) of two and four-phase models (dashed and solid lines, respectively). Reference frequency ω_o corresponds to (he. ${}_0S_2$ free oscillation. The hand is shown spans the entire range of long period tides and extends to 60 seconds ($\approx 10^5$ μHz) in the seismic range. Frame (a) shows experimental Q_μ determined at high temperature ($\geq 1000°C$) and pressure ($\approx$ 300 MPa for squares from *Jackson, Paterson & FitzGerald [1992]* using Aheim dunite **and** $\approx$ 20 MPa for stars from *Gueguen et* al. *[1989]* using single crystal forsterite). Seismicall y determined mantle Q_μ arc general ly factors of 2 to 10 larger that experimental values. The value of Q_μ at the Chandler wobble. period corresponds to that deduced by *Smith & Dahlen [1981]* and estimated parametrically by *Wilson & Vicente [1990]* (total bounds indicated by horizontal dashed lines). (Q_μ differs from solid Q of the Chandler wobble by a scale factor less than 1.8 *[Okubo 1982],* but here this is ignored since it is inconsequential to the basic effect being demonstrated). The cross shows the preferred value of *Wilson & Vicente* [1990] (see their model 11- 14). Tidal dispersion (measured by modeling k_2) is less than one percent for semi-diurnal (M_2) and 13.66 day (Mf) tidal frequencies *[Robertson, Ray & Carter 1994; Charles F. Yoder, personal communication]*. Refer to Table A-3 for viscosity ratio and concentration definitions **for** the **4** -phase composite. The long dashed line and staggered long-short arc contributions from phase.s in volume 2 and 1, respectively. These volume contributions **combine.** (see equations A-6, 7) to form the 4-phase material response (solid line). Also shown is a curve (shortest dash) in (b) for a 'power-law' with an exponent of *0.09 (scc* equation 7.4 of *Smith & Dahlen [1981])* and a reference frequency, ω_o, al ${}_0S_2$, consistent with the other curves. Note that the power-law anelastic model easily fits the Chandler wobble frequency (CW) estimates (cross) by shifting reference frequency, ω_o, well value above that for ${}_0S_{19}$. However, the latter model lacks structure: a factor which may prove crucial to fitting the entire band.

Figure 8. Same as Figure 7 except lower matrix viscosity ${}^{(1)}\eta$ and lower type (1) inclusion viscosity ${}^{(1)}\eta'$.

Figure A-1. Cartoon of a laterally heterogenous 4-phase viscosity mantle. Type (2) inclusions take. the shapes of spheres in the model discussed in the. Appendix,

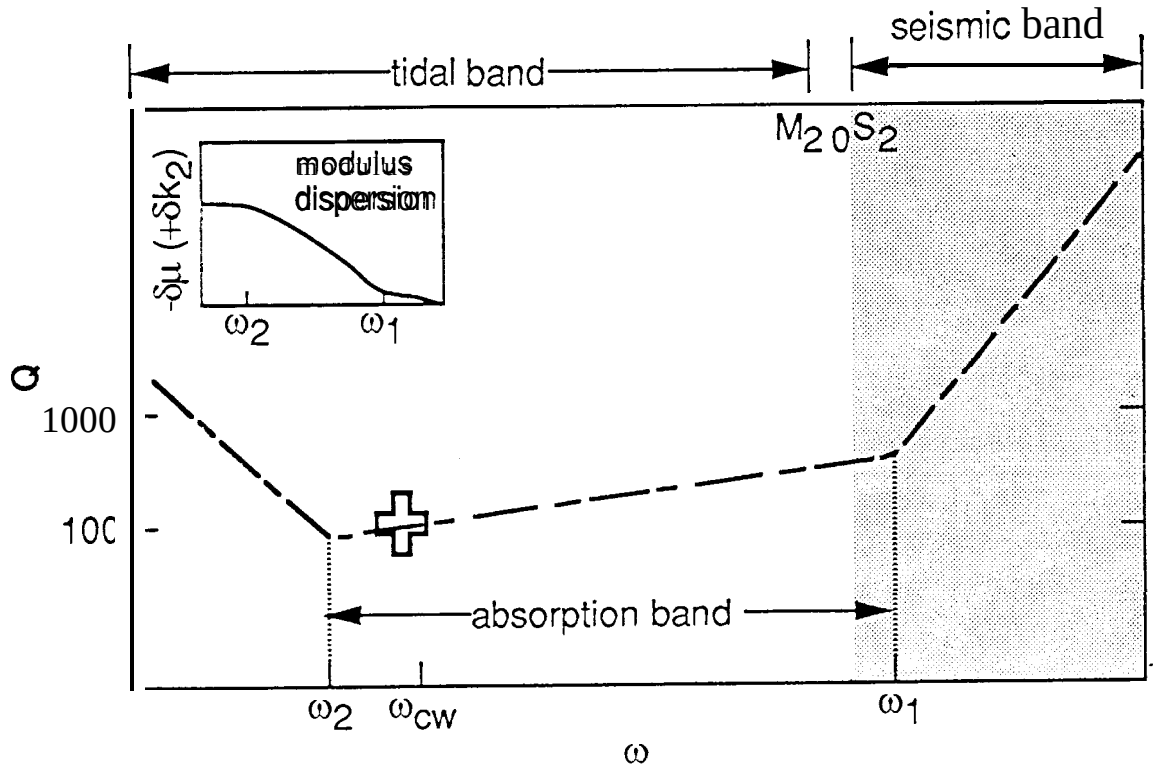
seismic band
tidal band
M_2 O_1 S_2
modulus dispersion
$-\delta\mu\ (+\delta k_2)$
ω_2
ω_1
Q
1000
100
absorption band
ω_2
ω_{cw}
ω_1
ω

Figure 1.

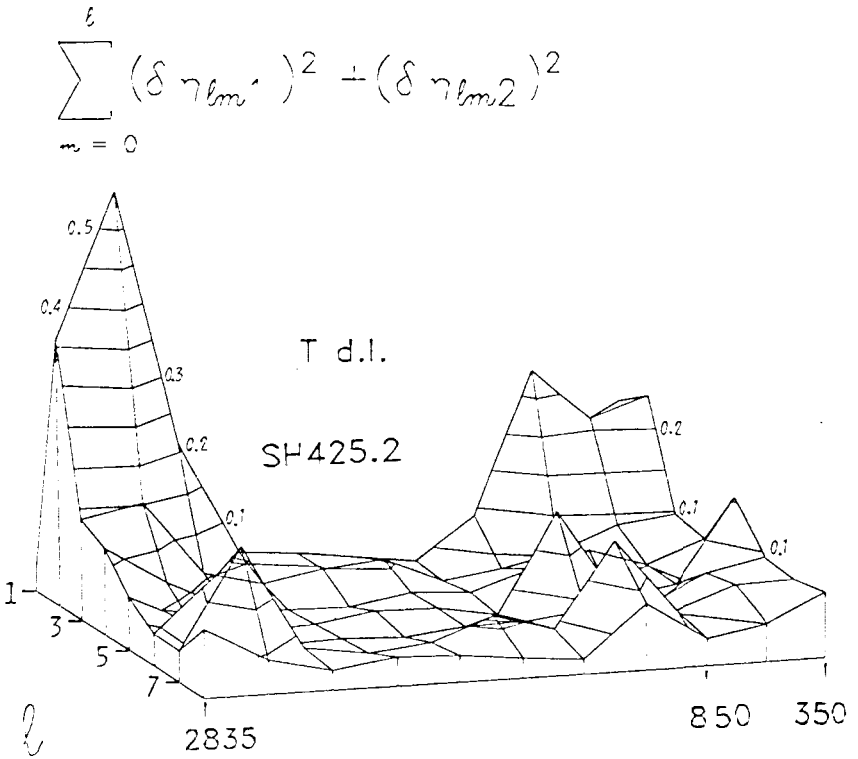
$\sum_{m=0}^{\ell} (\delta\eta_{\ell m1})^2 + (\delta\eta_{\ell m2})^2$
T d.l.
SH425.2
0.5
0.4
0.3
0.2
0.1
1
3
5
7
ℓ
2835
850
350

(a)

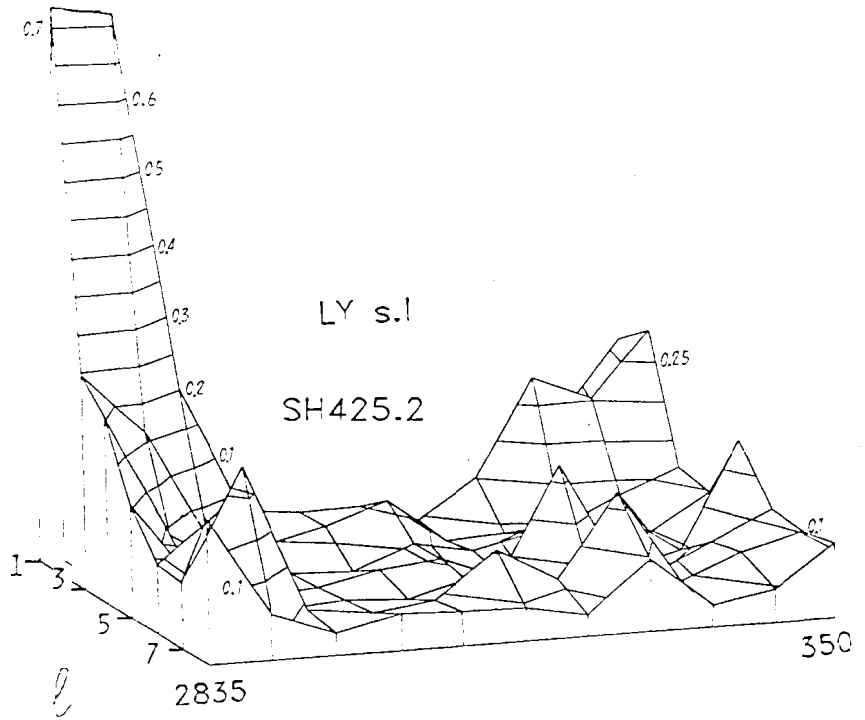
LY s.l
SH425.2
0.7
0.6
0.5
0.4
0.3
0.2
0.1
0.25
1
3
5
7
ℓ
2835
350

(b)

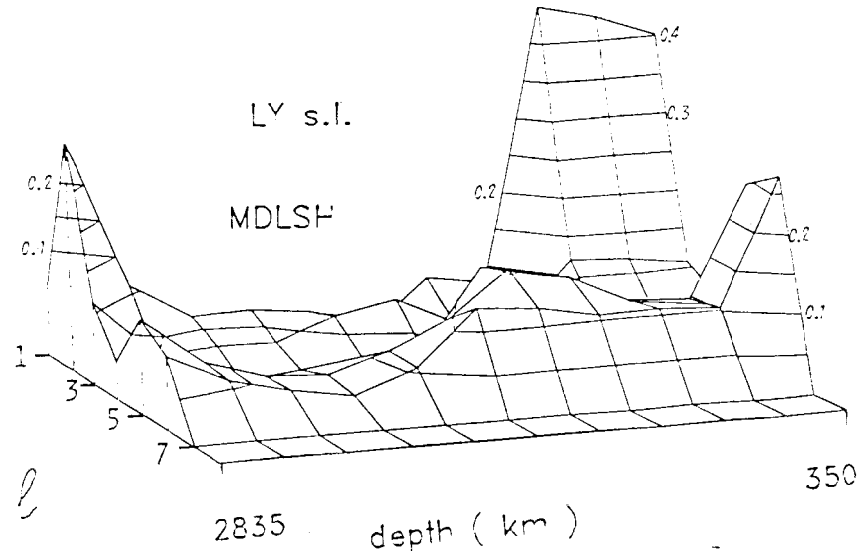
LY s.l.
MDLSH
0.4
0.3
0.2
0.1
1
3
5
7
ℓ
2835
depth (km)
350

(c)

Figure 2.

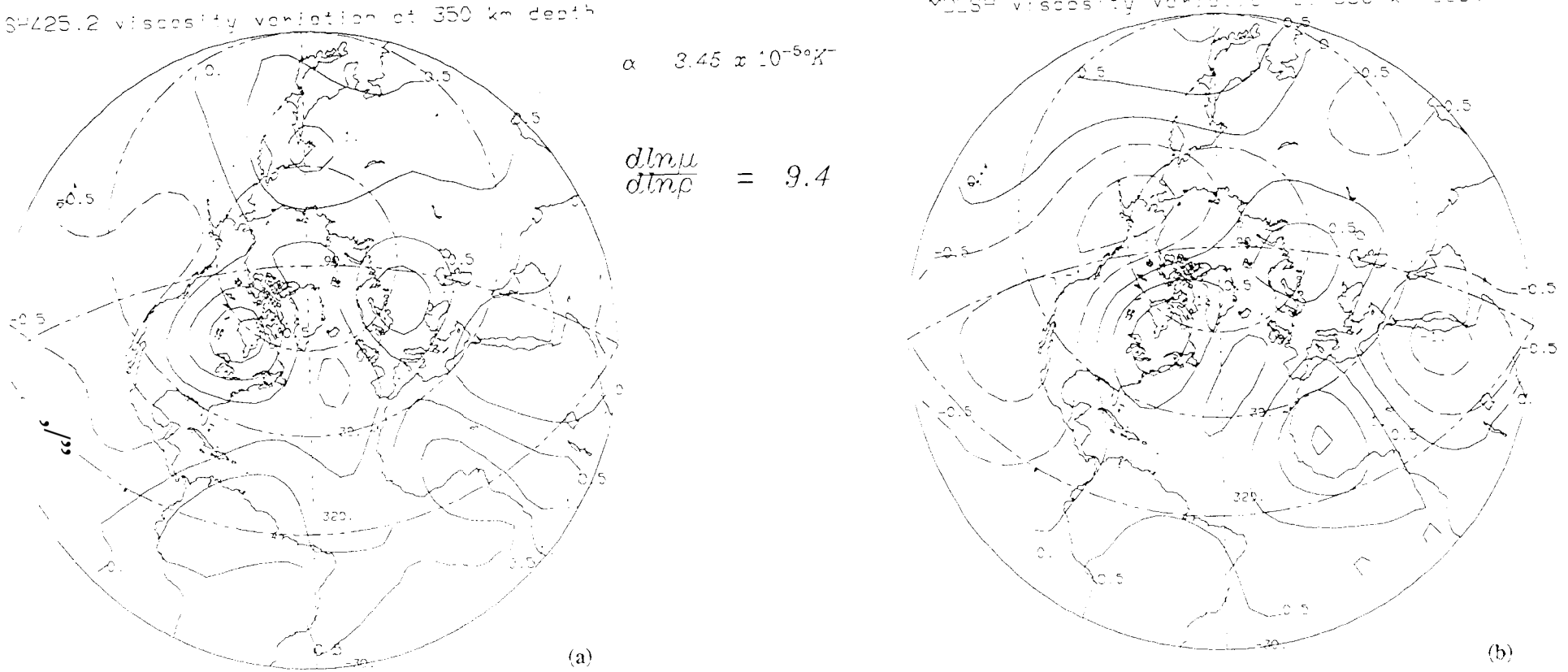
SH425.2 viscosity variation at 350 km depth
α 3.45 x 10⁻⁵°K⁻
dlnμ/dlnρ = 9.4
(a)
MDLSH viscosity variation at 350 km depth
(b)

Figure 3.

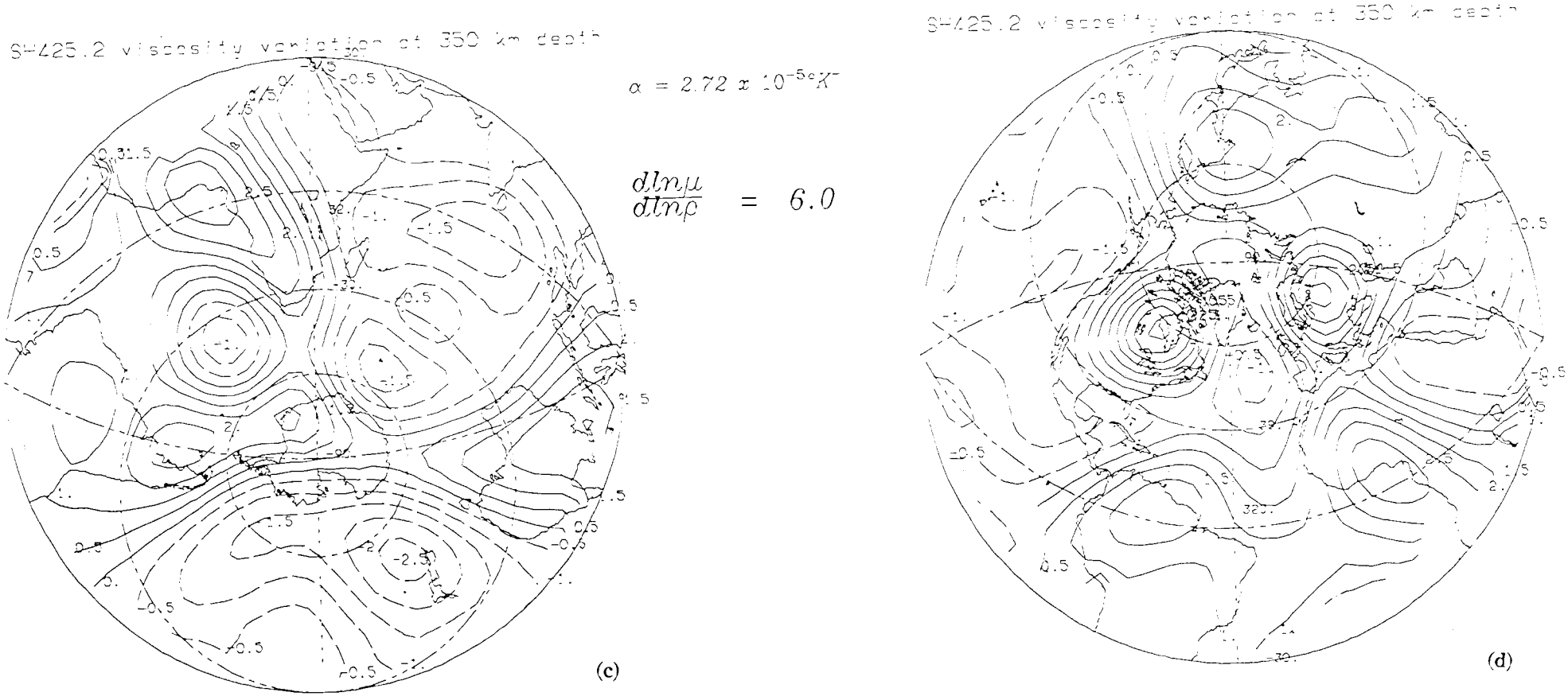
SH425.2 viscosity variation at 350 km depth
$\alpha = 2.72 \times 10^{-5} e^{X}$
$\frac{d\ln\mu}{d\ln\rho} = 6.0$
(c)
(d)

Figure 3.

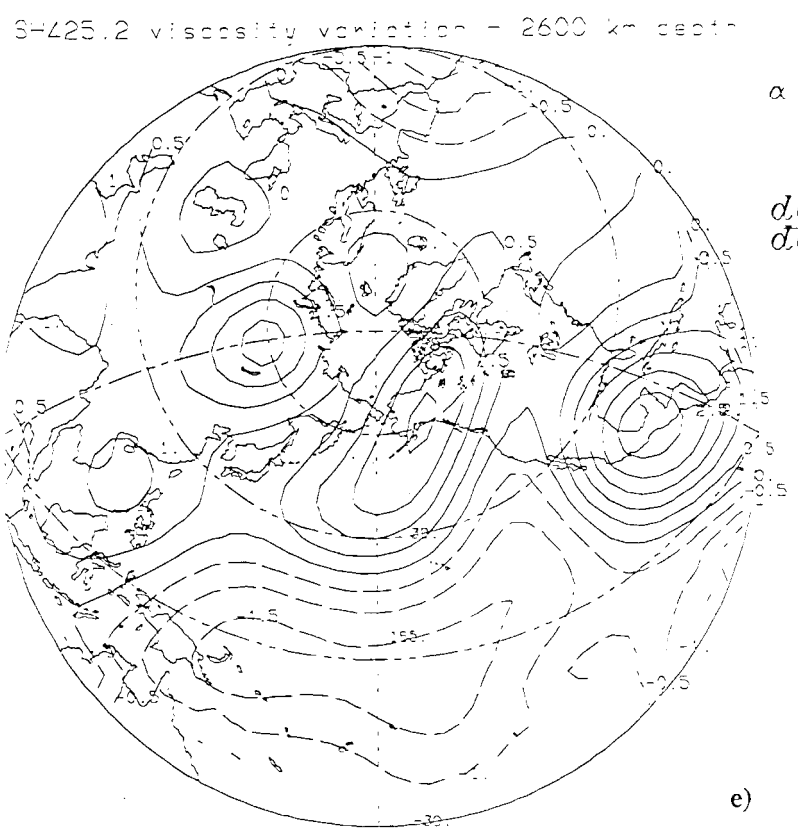

$\alpha \quad 0.90 \times 10^{-5} K^{-1}$

$$\frac{d\ln\mu}{d\ln\rho} = 9.4$$

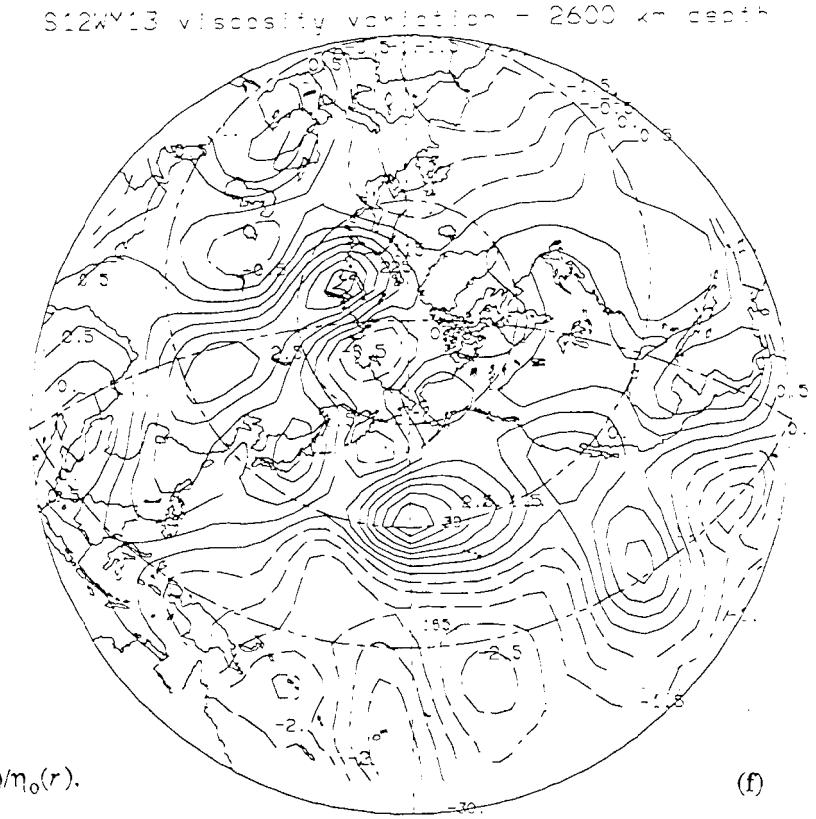

e)

$\Delta\eta(r,\theta,\lambda) \equiv \eta(r,\theta,\lambda)/\eta_o(r).$

(f)

Figure 3.

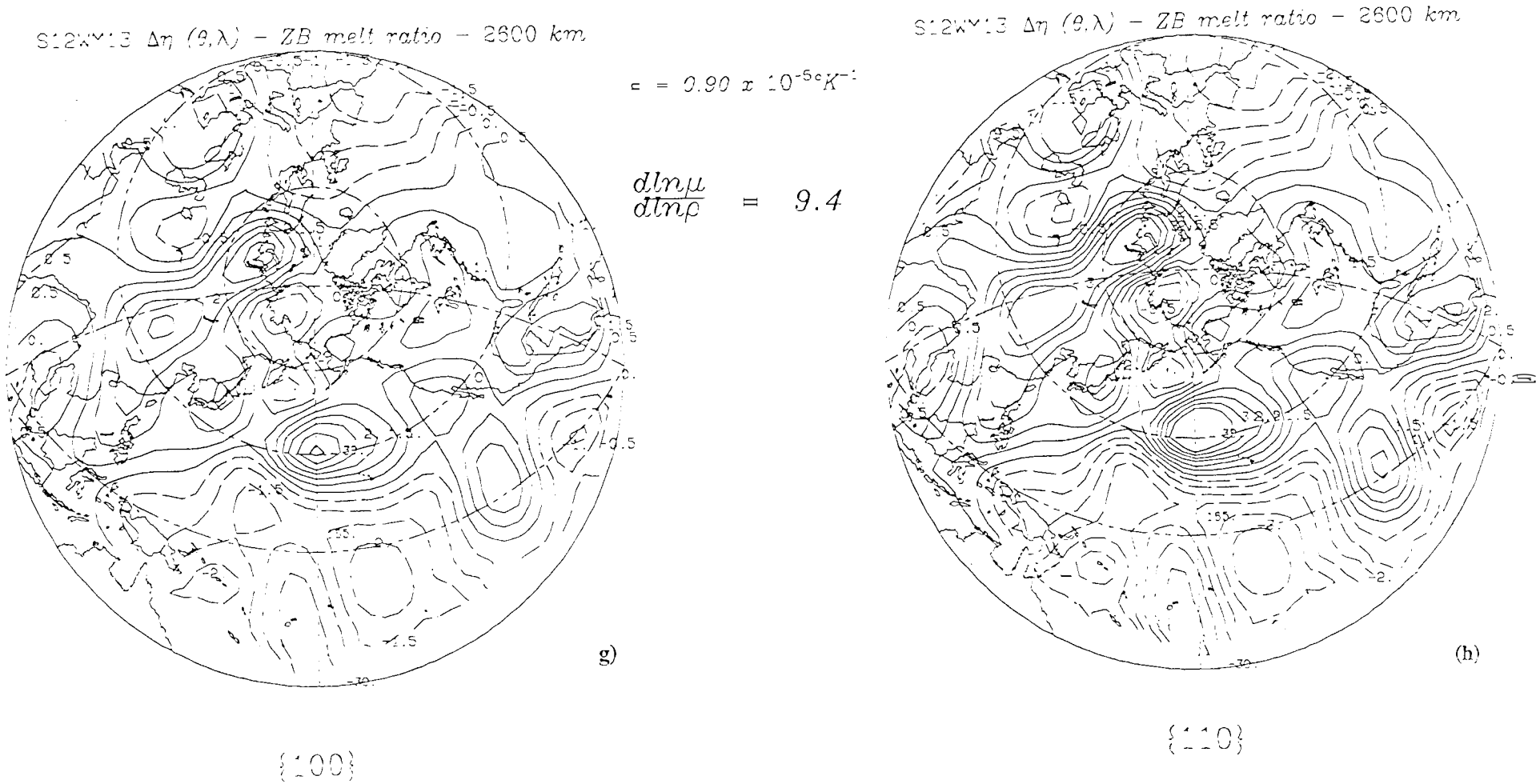
S12WY13 Δη (ϑ,λ) – ZB melt ratio – 2600 km
α = 0.90 x 10⁻⁵°K⁻¹
dlnμ / dlnρ = 9.4
g)
{100}
S12WY13 Δη (ϑ,λ) – ZB melt ratio – 2600 km
(h)
{110}

Figure 3.

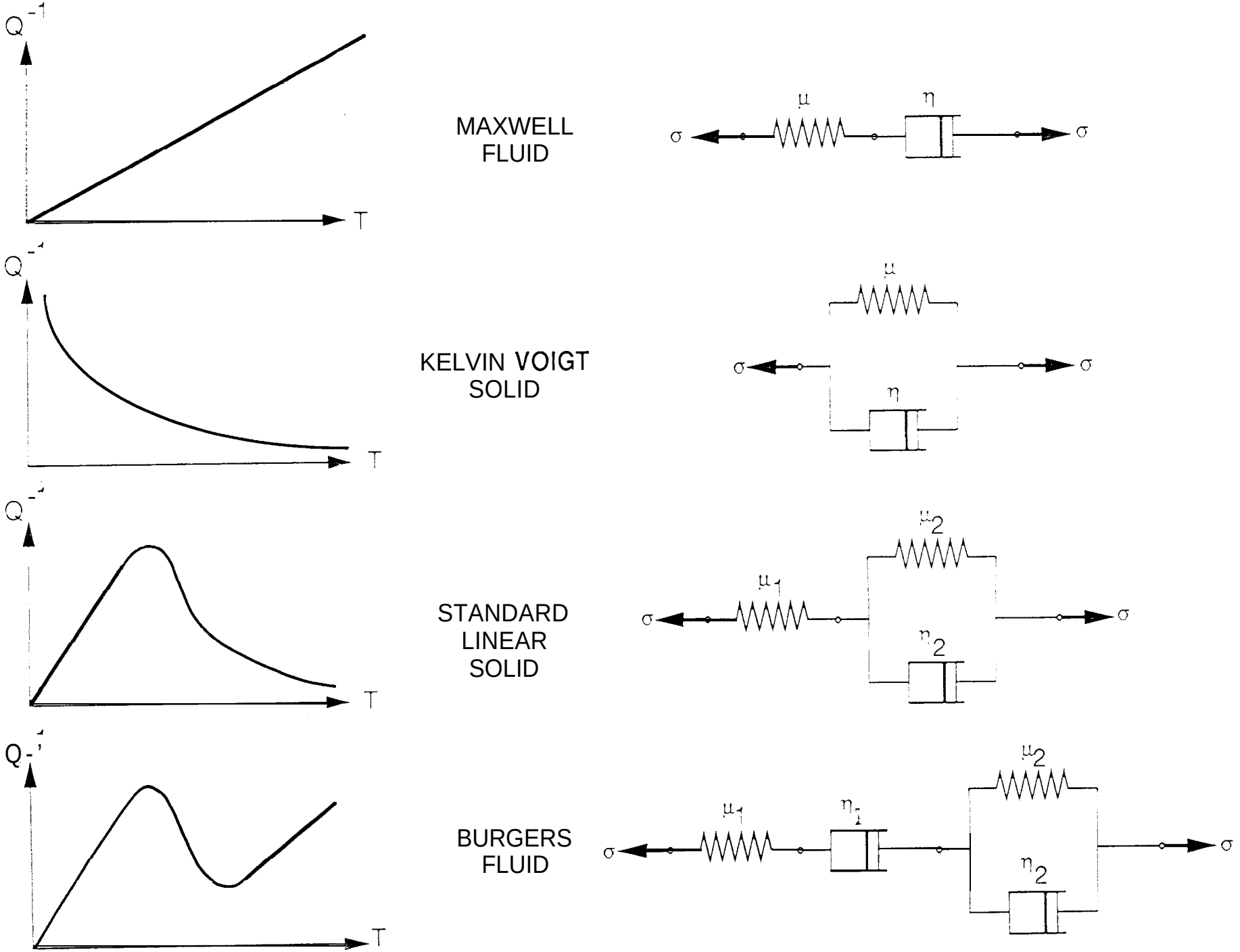
Q⁻¹
T
MAXWELL FLUID
μ
η
σ
σ
KELVIN VOIGT SOLID
STANDARD LINEAR SOLID
μ2
μ1
η2
BURGERS FLUID
η1

Figure 4.

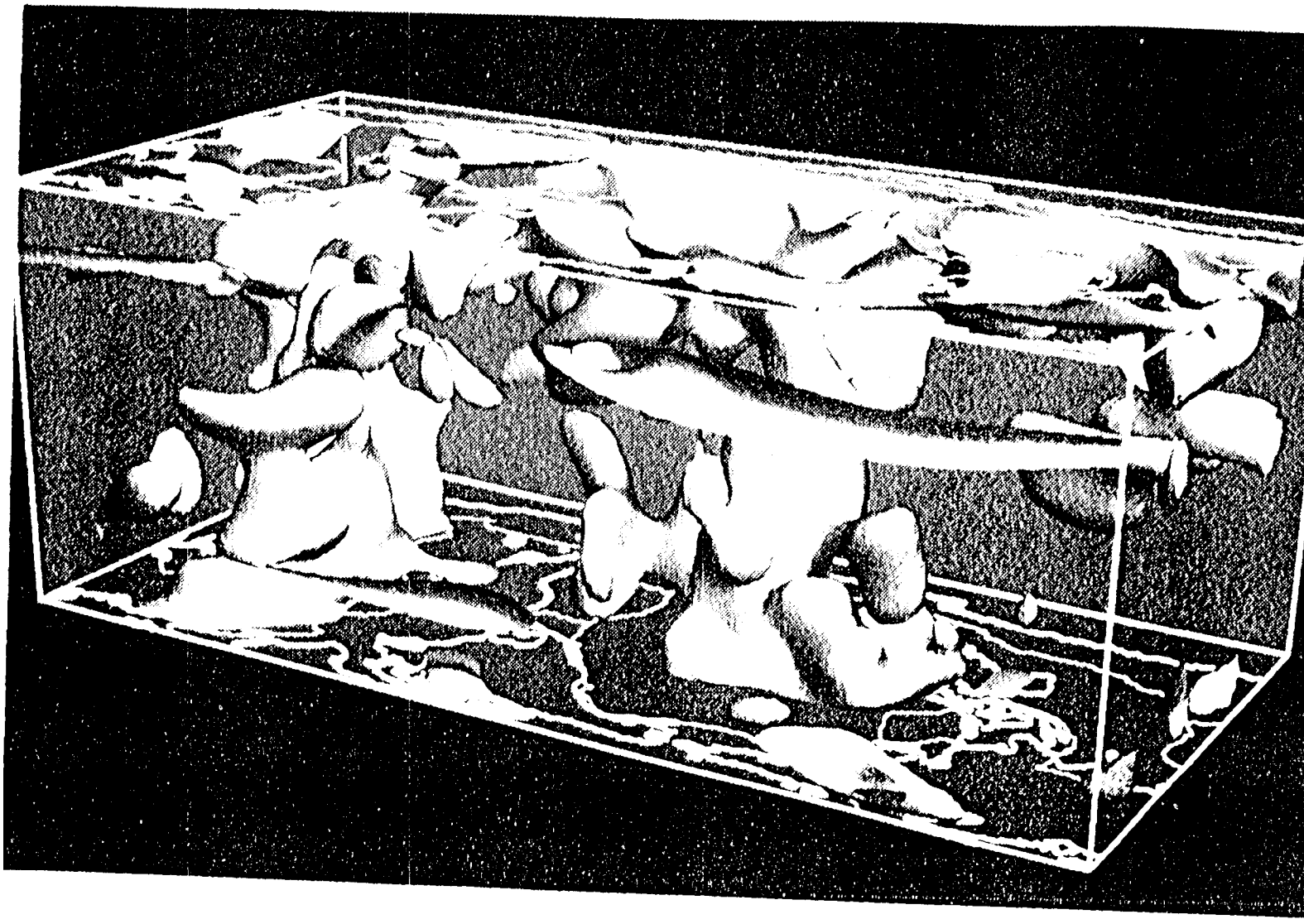

Figure 5.

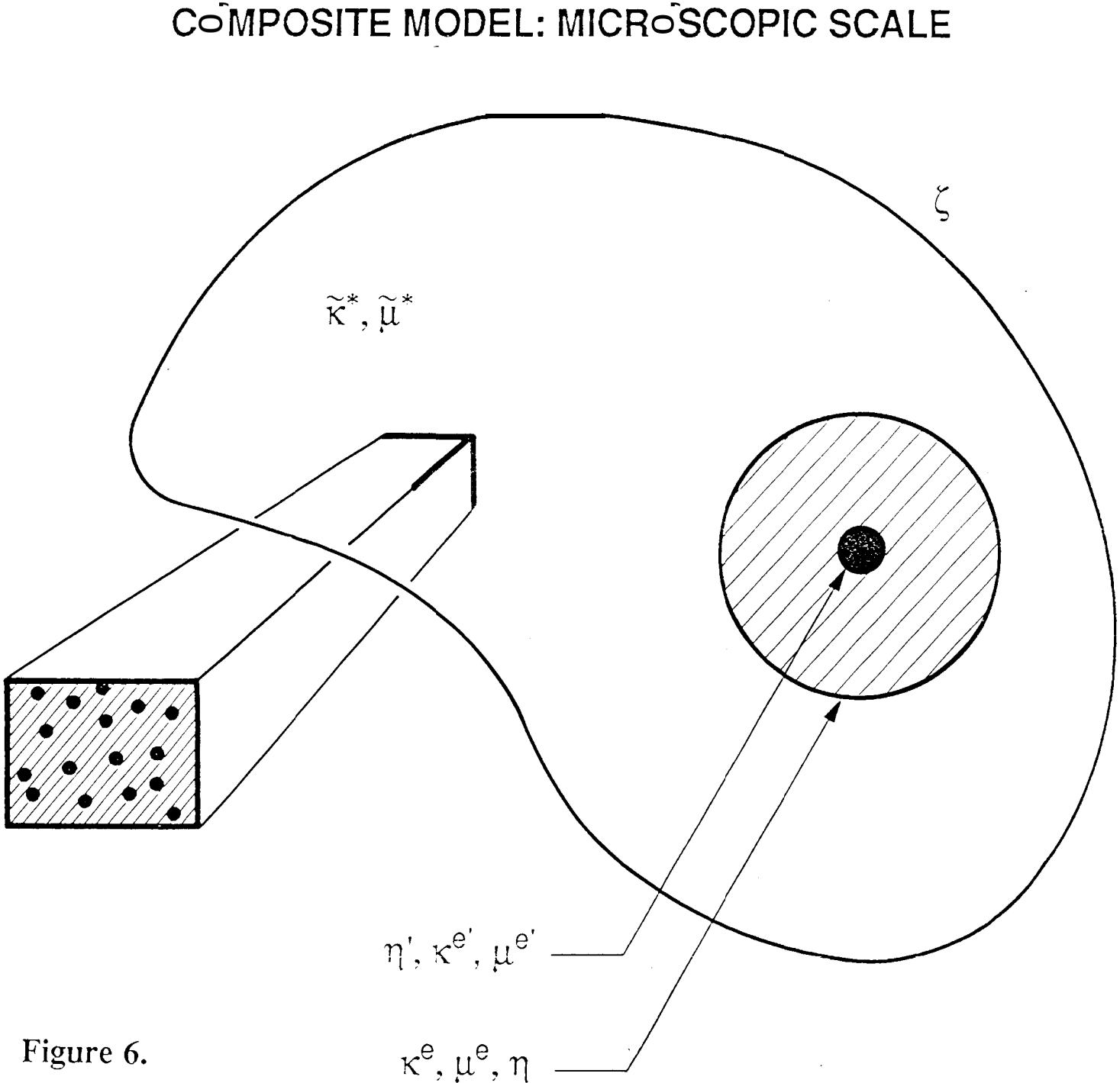
COMPOSITE MODEL: MICROSCOPIC SCALE
ζ
$\tilde{\kappa}^*, \tilde{\mu}^*$
$\eta', \kappa^{e'}, \mu^{e'}$
κ^e, μ^e, η

Figure 6.

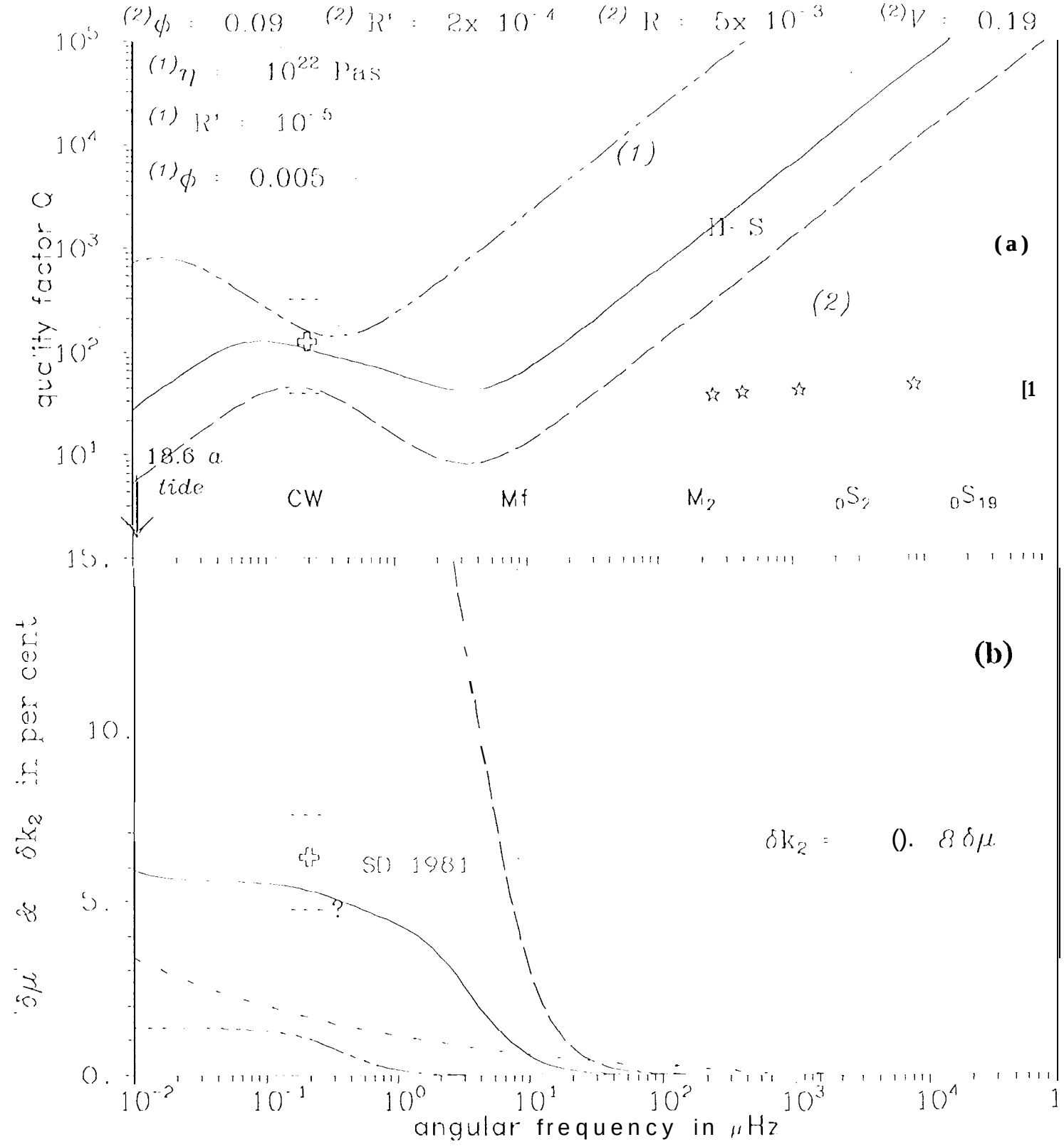
(2)φ = 0.09
(2) R' = 2x 10⁻⁴
(2) R = 5x 10⁻³
(2)V = 0.19
(1)η = 10²² Pas
(1) R' = 10⁻⁵
(1)φ = 0.005
(1)
(2)
M. S
(a)
[1
18.6 a
tide
CW
Mf
M2
0S2
0S19
quality factor Q
(b)
δk2 = 0. 8 δμ
SD 1981
δμ & δk2 in per cent
angular frequency in μHz

Figure 7.

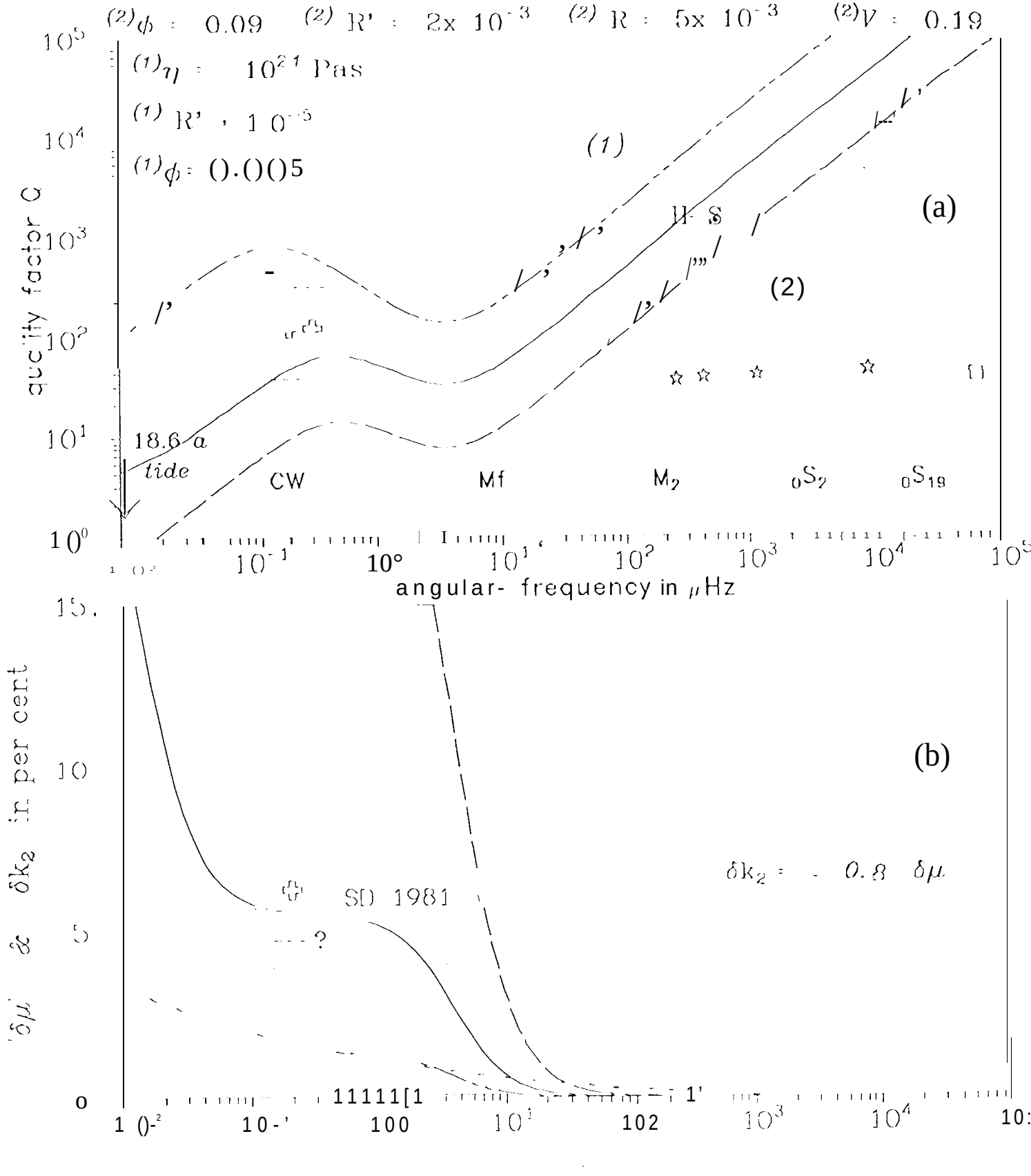
(2)φ = 0.09
(2) R' = 2x 10⁻³
(2) R = 5x 10⁻³
(2)V = 0.19
(1)η = 10²¹ Pas
(1) R' = 10⁻⁵
(1)φ = 0.0005
(1)
(2)
(a)
acuity factor Q
18.6 a
tide
CW
Mf
M2
0S2
0S19
angular- frequency in μHz
(b)
δμ & δk2 in per cent
δk2 = - 0.8 δμ
SD 1981
?

Figure 8.

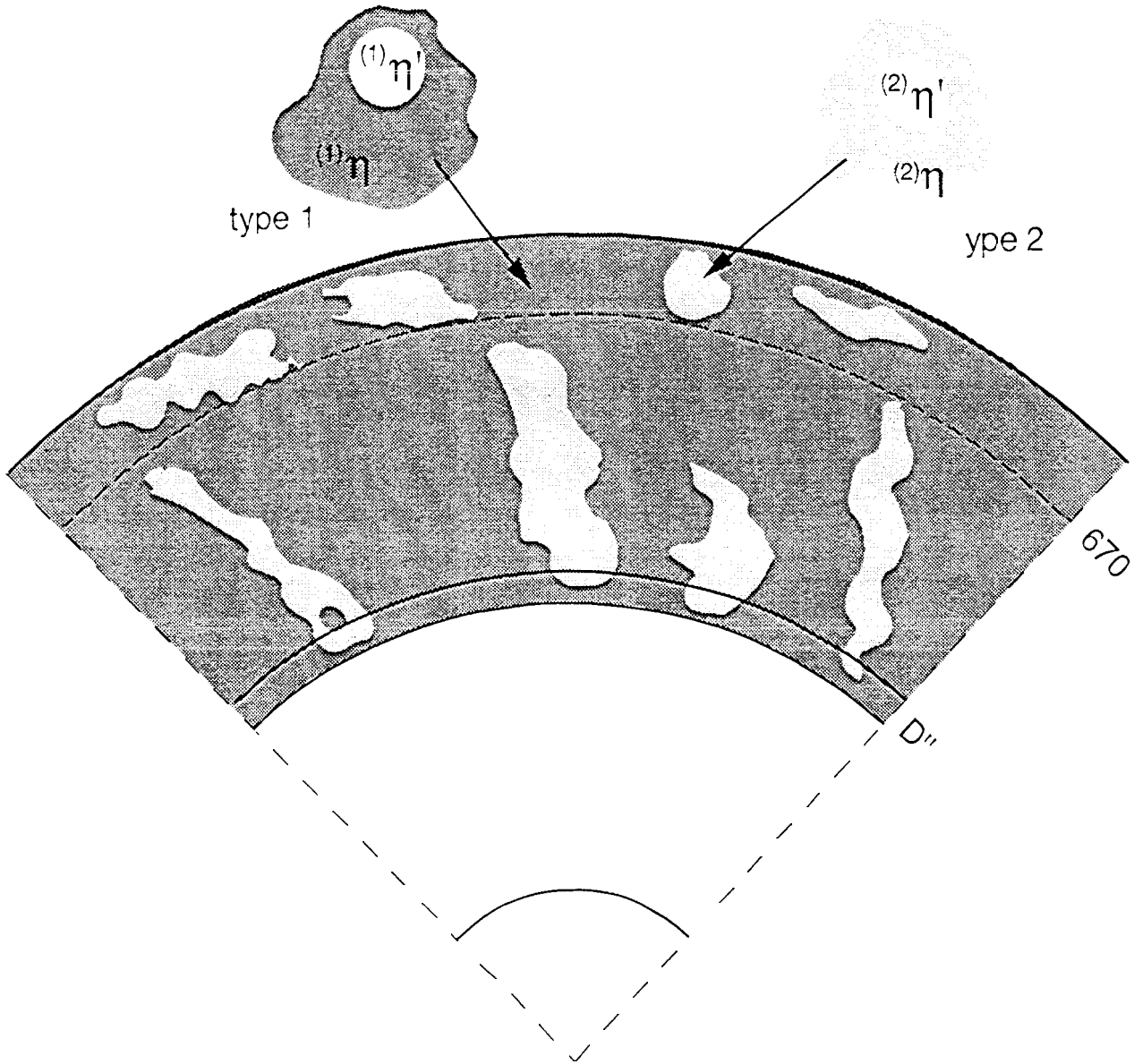

FOUR PHASE V SCOELASTIC M[illegible] MO[illegible]L

Table 1. Depth-dependent parameters used for calculating lateral viscosity power spectra.

depth (km)	A^* (10^2)	En/A^* †	T_0† (10^3 °K)	$T_{0.4}$ (10^3 °K)	a (10^4 °K)	α (10^{-5} °K^{-1})
350.	1.13	0.059	2.088	1.99	8.2	1.725
450.	1.22	0.052	2.069	2.1	8.3	1.65
550.	1.33	0.057	2.1	2,2	8.5	1.5
700.	1.11	0.064	2.3	2.23	8.3	1.463
900.	1,01	0.066	2.5	2.275	8.7	1.425
1 200.	1.10	0.064	2.6	2.296	9.35	1.3
1 500.	1.25	0.061	2.65	2.47	9.97	1.177
1803.	1.43	0.059	2.7	2.53	10.6	1.05
2200.	1.77	0.056	2.675	2.562	11.0	0.9
26a).	2.08	0,056	2.75	2.53	11.4	0.75
2835.	1.76	O.(M4	3.25	2.675	11.7	0.65

† Assumes intermittent double-layer convecting mean temperature calculated by *Tackley et al.* [1993]. $\varepsilon^* = \varepsilon\sqrt{\delta v_S / v_{S0}}$.

‡ Single-layer convecting mean temperature calculated by *Leitch and Yuen* [1989].

Table 2. Viscosity Ratios †.

Ratio	Definition
$\Lambda\eta$	$\eta(r,\theta,\lambda) / \eta_o(r)$
$\Lambda\bar{\eta}_i$	at concentration ϕ_i, ratio of weak to average of remaining heterogeneous viscosity
R	composite idealization of $\Lambda\bar{\eta}_i$

† See discussion in Sections 4 and 5

'1'able A-1. Coefficients for Two-phase Maxwell Viscoelastic Composite†

n	a_n
1	$\nu\left[(1+R) - \phi(1-R)\right]$
2	$\frac{1}{3}\left(\text{Ii}\ 7R\right) + \nu(1+3R) + \phi(1-R)(\frac{7}{3}+\nu)$
3	$2R\ .\ (\frac{4}{3}+\nu)$

n	b_n
1	$\nu\left[(1\text{-}1\ R) - \phi(1-R)\right]$
2	$\frac{1}{3}(\text{Ii}\ 7R) + \nu(1+3R) - (\$(1--R)(\frac{1}{3}+\nu)$
3	a_3

† Refer m Equations (A-1) m (A-4)

Table A-2. General Creep Function for 2D Composite Rheology†.

i	Decay Spectra λ_i
$\left\{ \begin{matrix} + \\ - \end{matrix} \quad \begin{matrix} fast \\ slow \end{matrix} \right\}$	$b_2 b_3^{-1} \left[\frac{1}{2} \pm \left(\frac{1}{4} - b_1 b_3 b_2^{-1} \right)^{\frac{1}{2}} \right]$

m	Θ_m
0	$\frac{b_2}{b_1} \left(1 - \frac{a_1}{b_1} \right) + \frac{a_3}{b_3}$
1	$\frac{a_1}{b_1}$
2	$\frac{1}{b_3 \lambda_{slow}^2 (\lambda_{slow} - \lambda_{fast})} \left[-a_1 + \left(b_2 + b_1 \frac{a_3}{b_3} \right) \lambda_{slow} - \left(b_3 + b_2 \frac{a_3}{b_3} \right) \lambda_{slow}^2 + a_3 \lambda_{slow}^3 \right]$
3	$\frac{1}{b_3 \lambda_{fast}^2 (\lambda_{slow} - \lambda_{fast})} \left[a_1 - \left(b_2 + b_1 \frac{a_3}{b_3} \right) \lambda_{fast} + \left(b_3 + b_2 \frac{a_3}{b_3} \right) \lambda_{fast}^2 - a_3 \lambda_{fast}^3 \right]$

†Refer to equations (A-1) to (A-4)

Table A-3. Components of 4-Phase Composite Viscoelastic Rheology †.

Parameter	Definition
$(1)_v$	type (1) 2-phase (matrix) concentration
$(2)''$	type (2) 2-phase (inclusion) concentration
$^{(2)}R$	$^{(2)}\eta / ^{(1)}\eta$
$^{(1)}\eta$	type (1) matrix viscosity
$^{(2)}\eta$	type (2) matrix viscosity
$^{(1)}R'$	$^{(1)}\eta' / ^{(1)}\eta$
$^{(2)}R'$	$^{(2)}\eta' / ^{(1)}\eta$
$^{(1)}\eta'$	type (1) inclusion viscosity
$^{(2)}\eta'$	type (2) inclusion viscosity
$^{(1)}\phi$	type (1) inclusion concentration
$^{(2)}A_L$	type (2) inclusion concentration

† Refer to Figures 6-8, A-1 and equations (A-6) to (A-9).